Sources and chemistry of nitrogen oxides over the tropical Pacific

Sources and chemistry of nitrogen oxides over the tropical Pacific

A. C. Staudt,[1,2] D. J. Jacob,[1] F. Ravetta,[1,3] J. A. Logan,[1] D. Bachiochi,[4]
T. N. Krishnamurti,[4] S. Sandholm,[5] B. Ridley,[6] H. B. Singh,[7] and B. Talbot[8]

Received 27 January 2002; revised 4 June 2002; accepted 19 November 2002; published 30 January 2003.

[1] We examine the sources and chemistry affecting nitrogen oxides ($NO_x = NO + NO_2$) over the tropical Pacific (30°S–20°N) using observations from the Pacific Exploratory Mission to the Tropics B (PEM-Tropics B) aircraft mission conducted in March–April 1999. A global model of tropospheric chemistry driven by assimilated meteorological data is used to interpret the observations. Median concentrations observed over the South Pacific during PEM-Tropics B were 7 pptv NO, 16 pptv peroxyacetyl nitrate (PAN), and 34 pptv nitric acid (HNO_3); the model generally reproduces these observations but overestimates those over the North Pacific. Lightning was the largest source of these species in the equatorial and South Pacific tropospheric column and in the tropical North Pacific upper troposphere. The oceanic source of acetone implied by high observations of acetone concentrations (mean 431 pptv) allows an improved simulation of PAN/NO_x chemistry. However, the high acetaldehyde concentrations (mean 78 pptv) measured throughout the troposphere are inconsistent with our understanding of acetaldehyde and PAN chemistry. Simulated concentrations of HNO_3 and HNO_3/NO_x are highly sensitive to the model representation of deep convection and associated HNO_3 scavenging. Chemical losses of NO_x during PEM-Tropics B exceed chemical sources by a factor of 2 in the South Pacific upper troposphere. The chemical imbalance, also apparent in the low observed HNO_3/NO_x ratio, is explained by NO_x injection from lightning and by frequent convective overturning which depletes HNO_3. The observed imbalance was less during the PEM-Tropics A campaign in September 1996, when aged biomass burning effluents over the South Pacific pushed the NO_x budget toward chemical steady state. *INDEX TERMS:* 0322 Atmospheric Composition and Structure: Constituent sources and sinks; 0365 Atmospheric Composition and Structure: Troposphere—composition and chemistry; 0368 Atmospheric Composition and Structure: Troposphere—constituent transport and chemistry; *KEYWORDS:* ozone, nitrogen oxides, troposphere, lightning, convection, tropics

Citation: Staudt, A. C., D. J. Jacob, F. Ravetta, J. A. Logan, D. Bachiochi, T. N. Krishnamurti, S. Sandholm, B. Ridley, H. B. Singh, and B. Talbot, Sources and chemistry of nitrogen oxides over the tropical Pacific, *J. Geophys. Res.*, *108*(D2), 8239, doi:10.1029/2002JD002139, 2003.

1. Introduction

[2] The capacity of the atmosphere to remove pollutants is largely dependent on the supply of oxidants in the troposphere [*Thompson*, 1992]. Nitrogen oxides (NO_x = NO + NO_2) are critical for generating ozone (O_3) and the hydroxyl radical (OH), the two most important tropospheric oxidants. Primary sources of NO_x to the troposphere include combustion, lightning, and microbial processes in soils [*Lamarque et al.*, 1996; *Lee et al.*, 1997]. These sources are almost exclusively from land. Because of its short lifetime against atmospheric oxidation (1–10 days), NO_x tends to be low over oceans. This depletion of NO_x over much of the troposphere limits the rate of O_3, and hence, OH production. The dominant sources of NO_x over oceans are thought to include long-range transport from continental source regions as well as chemical recycling of nitric acid (HNO_3) and peroxyacetyl nitrate (PAN) [*Moxim et al.*, 1996; *Penner et al.*, 1998]. Both HNO_3 and PAN can have lifetimes of weeks in the troposphere and therefore provide a secondary source of NO_x far from the point of original emission.

[3] We examine here the factors affecting NO_x concentrations over the remote tropical Pacific using observations obtained during the Pacific Exploratory Mission to the Tropics phase B (PEM-Tropics B), a NASA Global Tropo-

[1]Division of Engineering and Applied Sciences and Department of Earth and Planetary Sciences, Harvard University, Cambridge, Massachusetts, USA.
[2]Now at Board on Atmospheric Sciences and Climate, The National Academies/National Research Council, Washington, D. C., USA.
[3]Now at Service d'Aéronomie du CNRS/IPSL, Université Paris, Paris, France.
[4]Department of Meteorology, Florida State University, Tallahassee, Florida, USA.
[5]School of Earth and Atmospheric Sciences, Georgia Institute of Technology, Atlanta, Georgia, USA.
[6]National Center for Atmospheric Research, Boulder, Colorado, USA.
[7]NASA Ames Research Center, Moffett Field, California, USA.
[8]Complex Systems Research Center/Institute for the Study of Earth, Oceans, and Space, University of New Hampshire, Durham, New Hampshire, USA.

0148-0227/03/2002JD002139$09.00

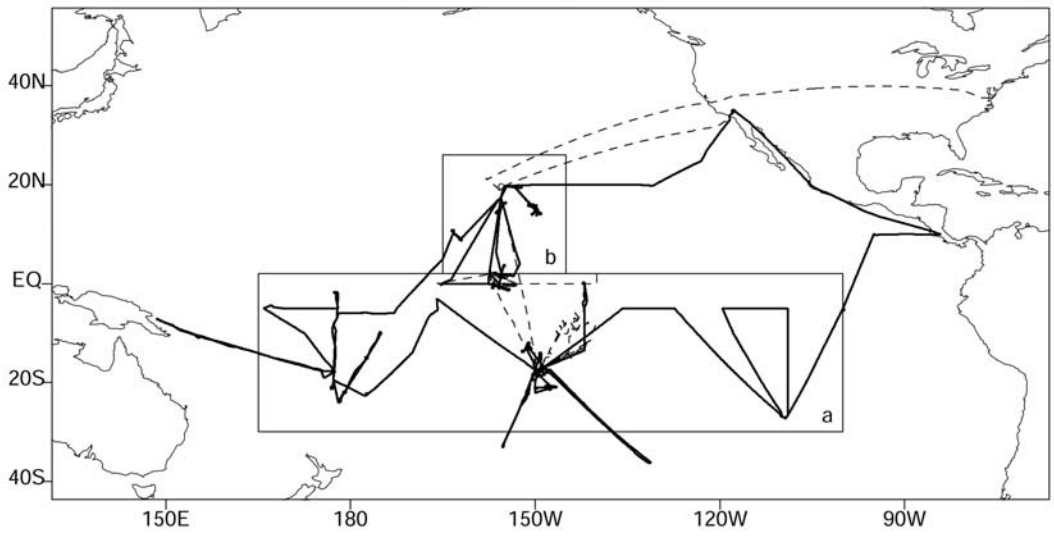

Figure 1. Map of PEM-Tropics B flight tracks. The heavy solid line shows the DC-8 tracks, and the dashed line shows the P-3B tracks. The observations are averaged over two regions for model evaluation and budget calculations: region a, tropical South Pacific, and region b, tropical North Pacific.

spheric Experiment (GTE) aircraft campaign conducted in March–April 1999 [*Raper et al.*, 2001]. The campaign employed two aircraft, a DC-8 and a P-3B, outfitted with instruments to measure O_3, hydrogen oxide radicals (HO_x = OH + HO_2), NO_x, HNO_3, PAN, CO, hydrocarbons, and a large number of related species. Operating out of Hawaii, Christmas Island, Fiji, Tahiti, and Easter Island, flights during PEM-Tropics B extensively surveyed the Pacific from 40°S to 40°N with numerous vertical profiles (flight tracks are shown in Figure 1). The PEM-Tropics B data complement observations obtained during previous GTE campaigns over the Pacific, in particular PEM-Tropics A [*Hoell et al.*, 1999], which surveyed a similar domain during August–September 1996. We interpret the PEM-Tropics B observations with a global 3-D chemical transport model driven by assimilated meteorological observations to assess the importance of primary sources and chemical recycling in controlling the abundance of NO_x in the region.

[4] Previous analyses of the PEM-Tropics A observations identified some of the factors determining the NO_x budget over the South Pacific in austral spring, when biomass burning in the Southern Hemisphere is at its seasonal maximum. *Schultz et al.* [1999] used a photochemical box model constrained with PEM-Tropics A observations to show that decomposition of PAN originating from biomass burning accounted for most of the NO_x in the lower troposphere (below 6 km). The NO_x budget in the upper troposphere during PEM-Tropics A was found by *Schultz et al.* [1999, 2000] to deviate from chemical steady state by a factor of 2–5 as diagnosed by the ratio LNO_x/PNO_x of chemical loss of NO_x (LNO_x) to chemical production (PNO_x), computed with their photochemical model. With a global 3-D model, *Staudt et al.* [2002] found that transport and subsidence of NO_x produced by lightning over the equatorial Pacific warm pool was responsible for perturbing the NO_x budget in the upper troposphere during PEM-Tropics A away from chemical steady state.

[5] Concentrations of NO_x, HNO_3, and PAN observed in the upper troposphere over the South Pacific during PEM-Tropics B were a factor of 2–3 less than those observed during PEM-Tropics A. PEM-Tropics B was conducted in the wet season of the southern tropics, when biomass burning is minimum. Using a photochemical box model to analyze the PEM-Tropics B observations, *Olson et al.* [2001] calculated a LNO_x/PNO_x of 2.0–3.3, similar to *Schultz et al.* [1999, 2000] for PEM-Tropics A. Likewise, *Wang et al.* [2001] found in a 1-D model for the PEM-Tropics B conditions that a large primary source of NO_x was needed in the middle and upper troposphere to explain the surplus of PAN and HNO_3 relative to NO_x. We will examine this issue further here using the capability of our global 3-D model to explicitly resolve the primary sources of NO_x during PEM-Tropics B.

[6] A number of global 3-D models have been applied previously to the investigation of NO_x in the remote troposphere, and have had some success in reproducing observed PAN and NO_x concentrations [*Singh et al.*, 1998; *Levy et al.*, 1999; *Emmons et al.*, 1997; *Thakur et al.*, 1999; *Bey et al.*, 2001a, 2001b; *Staudt et al.*, 2002]. A general result from these models is that decomposition of PAN is the principal source of NO_x in much of the remote troposphere. This result is sensitive to the abundances of acetaldehyde (CH_3CHO) and acetone, the prinicipal precursors responsible for conversion of NO_x to PAN. PEM-Tropics B included the first extensive measurements of CH_3CHO and acetone in the Pacific troposphere, and these indicated concentrations higher than would be expected from current models by a factor of 3 or more [*Singh et al.*, 2001]. Such a model underestimate could challenge the conventional view of the importance of PAN as a source of NO_x in the remote troposphere. We will examine this issue in this paper.

[7] PEM-Tropics B included a number of flights over the northern tropical Pacific out of Hawaii, in contrast to PEM-Tropics A, which focused on the South Pacific. Observations

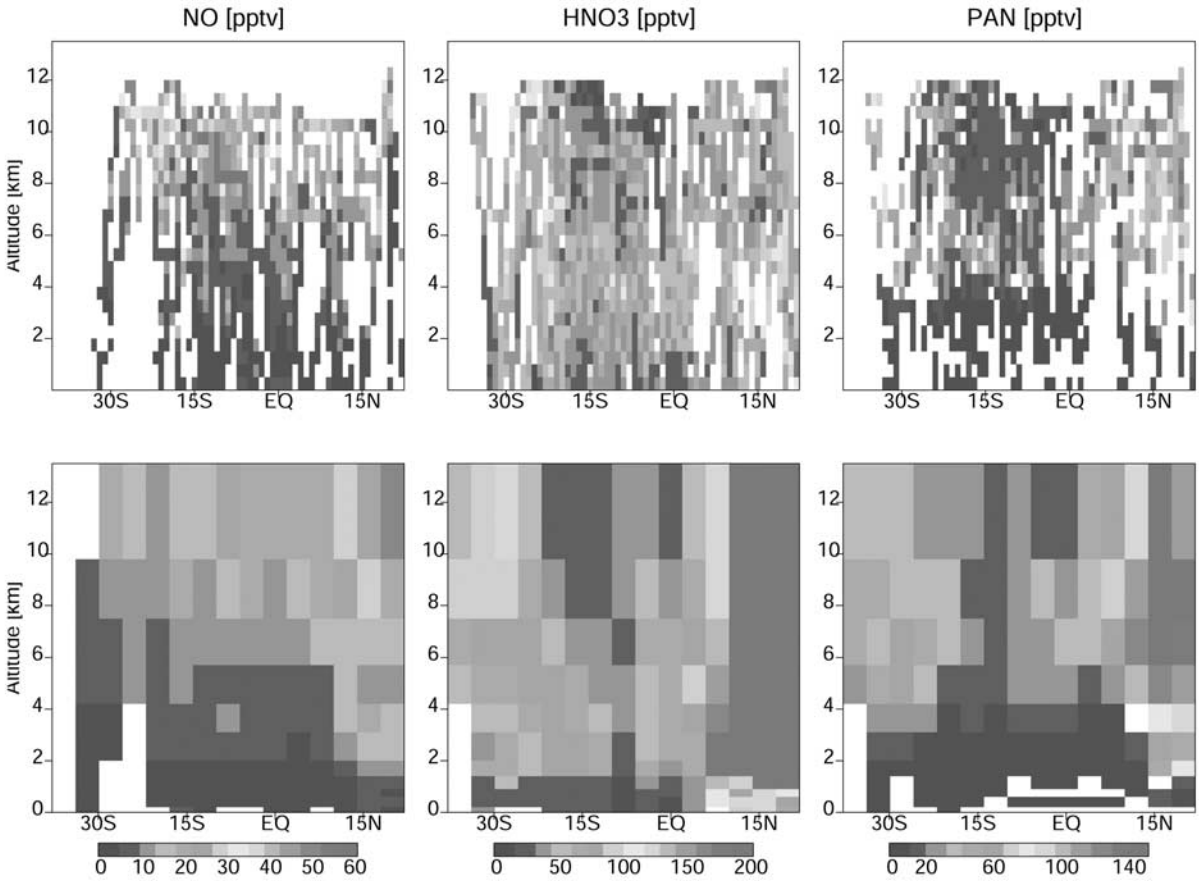

Figure 2. Concentrations of NO, HNO_3, and PAN during PEM-Tropics B plotted as a function of altitude and latitude (see Figure 1). (top) Observations averaged across 165°E–100°W longitude and into 0.5° latitude by 0.5 km altitude boxes. The NO observations have been restricted to those obtained between 0900 and 1500 LT. (bottom) Simulated concentrations of NO, HNO_3, and PAN sampled for the day and location of the PEM-Tropics B flights. The model values are sampled along the flight tracks and for the flight days, and the results are averaged across 165°E–100°W longitude and for the model resolution of 4° latitude. The simulated NO is the average of daytime (0900 to 1500 LT) concentrations, while HNO_3 and PAN are 24-hour averages. DC-8 flight 22, which followed the western coast of Central America from Costa Rica to California, is not included. See color version of this figure at back of this issue.

of CO, hydrocarbons, and halocarbons in that region indicated considerable combustion influence, with fossil fuel sources from Eurasian sources dominating in the boundary layer and biomass burning sources from Southeast Asia dominating in the free troposphere [*Blake et al.*, 2001; *Staudt et al.*, 2001]. Biomass burning in the northern tropics (including Southeast Asia and the Indian subcontinent) was at its seasonal maximum during PEM-Tropics B. We will examine here the importance of these sources in determining the concentrations of NO_x over the northern tropical Pacific, particularly in relation to lightning, which was found in previous global model studies to be the principal source of NO_x in the region [*Levy et al.*, 1999; *Tie et al.*, 2001].

2. PEM-Tropics B Meteorological and Chemical Environment

[8] As shown in Figure 1, the PEM-Tropics B aircraft sampled extensively the troposphere above the tropical Pacific. Transport to this region was governed by semi-permanent subtropical high pressure systems located above the northeast and southeast Pacific, which bring air from midlatitudes toward the equator, feeding into the easterly flow of the trade winds [*Merrill*, 1989]. Major barriers to horizontal air flow were the Intertropical Convergence Zone (ITCZ) and the South Pacific Convergence Zone (SPCZ) [*Fuelberg et al.*, 2001]. The ITCZ was less defined than on average over the Pacific during PEM-Tropics B because of normal seasonal variability amplified by the strong La Nina conditions at the time [*Fuelberg et al.*, 2001]. La Nina conditions also shifted the SPCZ westward of its typical position [*Fuelberg et al.*, 2001]. This shift created a window in the vicinity of the dateline where northern hemispheric air could travel into the Southern Hemisphere near the surface. Transport of northern hemispheric midlatitude anthropogenic effluents around the North Pacific High into the trade winds and through this window has been termed the "river of pollution" [*Staudt et al.*, 2001].

[9] Figure 2 (top) shows the observed distributions of NO, HNO_3, and PAN as a function of latitude and altitude during PEM-Tropics B. Longitudinal variations were relatively small. The observations have been averaged across all longitudes and into 0.5° latitude by 0.5 km altitude boxes. The nitrogen oxide radicals (NO and NO_2) were measured on the DC-8 using the photofragmentation two-photon laser-induced fluorescence technique [*Bradshaw et al.*, 1999]. The NO_2 concentrations measured by this method have been shown to match closely the expected photochemical equilibrium with NO [*Bradshaw et al.*, 1999; *Schultz et al.*, 1999]. On the P-3B, NO and NO_2 were measured by chemiluminescence using a method similar to that described by *Ridley et al.* [2000]. We focus here on the measurements of NO, which were made with greater precision. Nitric acid was measured with a mist chamber technique [*Talbot et al.*, 1999], with temporal resolution ranging from 4 min near the surface to 8 min in the upper troposphere. Peroxyacetyl nitrate was measured on the DC-8 aircraft only, using gas chromatography with electron capture detection from a cryogenically enriched sample of ambient air [*Singh et al.*, 2001]. Eighty percent of the PAN observations below 1 km altitude were below the 1 pptv limit of detection [*Olson et al.*, 2001].

[10] The observations of NO in the Southern Hemisphere show a strong vertical gradient with higher concentrations in the upper troposphere (Figure 2). From the surface up to 4–6 km altitude, NO concentrations were generally less than 5 pptv. Enhanced NO concentrations at altitudes greater than 9 km above the southern and equatorial Pacific were likely the result of lightning, which was active in the warm pool area of the southwest equatorial Pacific, but also more generally over the South Pacific [*Fuelberg et al.*, 2001]. Somewhat lower NO concentrations were observed in the upper troposphere above the North Pacific (Figure 1), which was more distant from areas of active convection and lightning.

[11] Low concentrations of HNO_3 were observed in the marine boundary layer above the southern and equatorial Pacific, reflecting deposition and uptake by sea salt (J. E. Dibb et al., Soluble N and S relationships in the equatorial Pacific, submitted to *Journal of Geophysical Research*, 2001, hereinafter referred to as Dibb et al., submitted manuscript, 2001). Nitric acid was also depleted in the upper troposphere at 15°S–10°N, due to the efficient scavenging in convective updrafts [*Mari et al.*, 2003]. Nitric acid concentrations in the upper troposphere increased south of 20°S due to less active convection. The highest concentrations of HNO_3 were sampled in the lower troposphere of the northern subtropics, where other tracers indicated a strong Eurasian pollution influence [*Staudt et al.*, 2001; *Blake et al.*, 2001]. Bulk filter measurements of aerosol nitrate (NO_3^-) during PEM-Tropics B (Dibb et al., submitted manuscript, 2001) had relatively sparse spatial coverage and were frequently below the limit of detection (typically 7–17 pptv). As shown in Figure 3, the ratio of total nitrate ($HNO_{3(gas)} + NO_{3\,(aerosol)}^-$) to $HNO_{3(gas)}$ was typically 1–2 for the ensemble of data where NO_3^- concentrations were above the detection limit.

[12] Observed PAN concentrations generally increased with altitude (Figure 2), reflecting the strong temperature dependence of PAN loss. Concentrations were less than 10 pptv throughout the lower troposphere. In equatorial regions, rapid convective mixing of air between the boundary layer and the free troposphere depressed PAN concentrations throughout the column. At 10–20°S, PAN concentrations in the upper troposphere were generally less than 20 pptv while midtropospheric (4–8 km altitude) concentrations were higher, suggesting a strong coupling between the lower and upper troposphere by deep convection. PAN was elevated in the middle and upper troposphere of the northern subtropics, reflecting biomass burning outflow from the Indian subcontinent and Southeast Asia as seen for other tracers [*Staudt et al.*, 2001; *Blake et al.*,

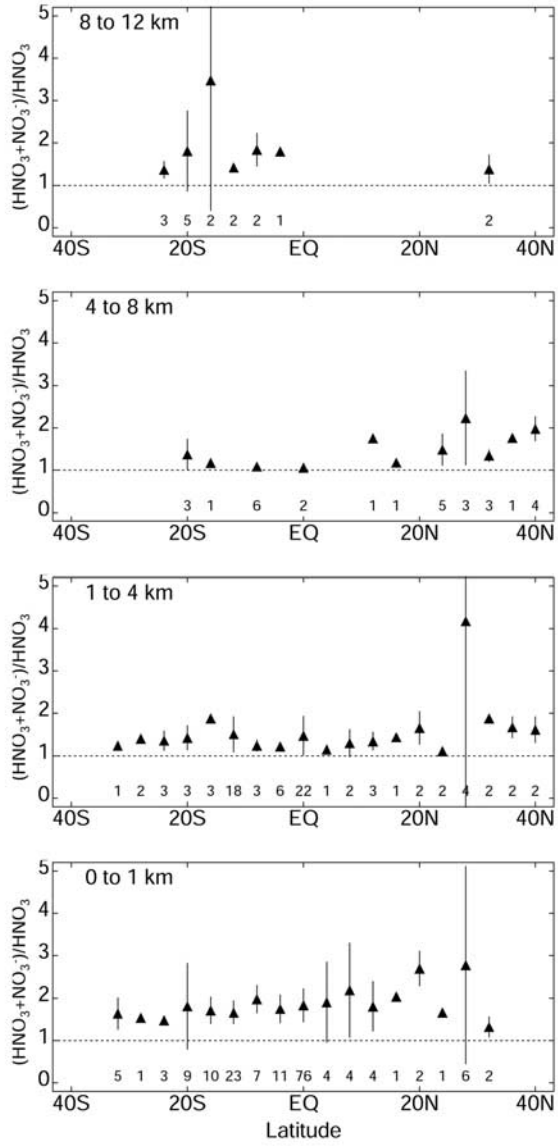

Figure 3. Latitudinal gradients of the concentration ratio [HNO_3(gas) + NO_3^- (aerosol)]/[HNO_3(gas)] observed during PEM-Tropics B. The observations are averaged over 1 March to 19 April 1999, 150°E–90°W longitude, the specified altitude ranges, and 4° latitude bins. Vertical bars indicate standard deviations. NO_3^- measurements below the limit of detection are not included.

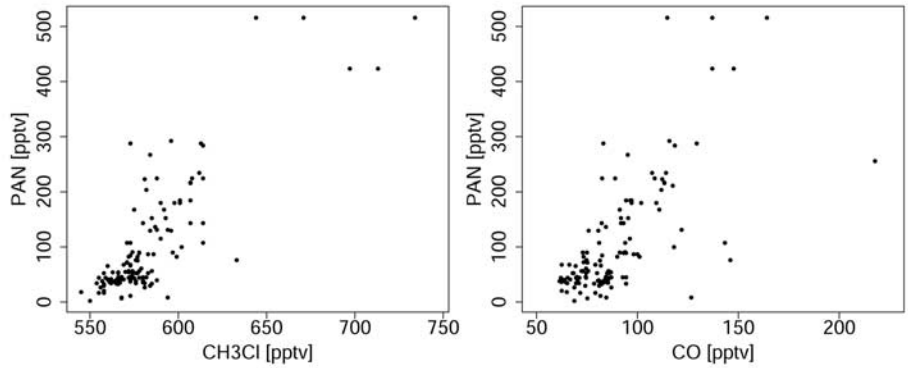

Figure 4. Relationship of PAN with CH_3Cl and CO during PEM-Tropics B over the North Pacific (north of 2°N) at 2–8 km altitude.

2001]. Indeed, PAN concentrations observed at 4–8 km altitude over the North Pacific were well correlated with CH_3Cl and CO, tracers of biomass burning (Figure 4).

[13] The concentrations of NO_x, HNO_3, and PAN observed over the tropical South Pacific (10–30°S) during PEM-Tropics B were a factor of 2 or more lower than those observed during PEM-Tropics A when a pervasive biomass burning influence was present, as illustrated in Table 1 [also see *Talbot et al.*, 2000]. Over the equatorial Pacific, the difference is less because biomass burning influence during PEM-Tropics A was largely confined south of 10°S [*Gregory et al.*, 1999]. Concentrations of NO and PAN in the lower troposphere over the equatorial Pacific were actually higher during PEM-Tropics B, when the river of Eurasian pollution [*Staudt et al.*, 2001] carried northern midlatitude effluents as far south as the SPCZ. During PEM-Tropics B, HNO_3/NO_x concentration ratios in the upper troposphere above the South Pacific were a factor of 3 less than those observed during PEM-Tropics A, indicating a larger chemical imbalance in the NO_x budget for this region.

3. Global 3-D Chemical Transport Model

[14] We use the Harvard/Florida State University (FSU) global chemical transport model (CTM) to investigate the factors affecting tropospheric NO_x over the remote Pacific during March–April 1999. This model has been previously applied to simulate tropospheric O_3-NO_x-hydrocarbon chemistry during PEM-Tropics A [*Staudt et al.*, 2002], to simulate sources and transport of CO during PEM-Tropics B [*Staudt et al.*, 2001], and to evaluate our understanding of the sources of oxygenated organics during PEM-Tropics B [*Singh et al.*, 2001]. It is driven by assimilated meteorological fields produced by the FSU Global Spectral Model [*Krishnamurti et al.*, 1993, 1996] for 22 January to 19 April 1999. A detailed treatment of tropical dynamics makes the FSU analysis especially useful for studies of the tropical Pacific. In particular, the precipitation rates used in the physical initialization process are derived from satellite observations of outgoing long-wave radiation and precipitation [*Krishnamurti et al.*, 1983; *Gairola and Krishnamurti*, 1992]. The CTM has 14 vertical layers along sigma coordinates (centered at 0.99, 0.95, 0.9, 0.85, 0.8, 0.7, 0.6, 0.5, 0.4, 0.3, 0.2, 0.1, 0.07, 0.03) and a horizontal resolution of 4° latitude by 5° longitude.

[15] Transport processes in the model include grid-scale advection using a second-order moments scheme [*Prather*, 1986], dry convection which redistributes tracer uniformly up to the mixed layer height calculated by the FSU model, and deep moist convection using convective mass fluxes diagnosed in the FSU model as described by *Staudt et al.* [2001]. Because the deep convective adjustment process in the FSU model is not easily adapted to tracer transport, the convective mass fluxes are not used in the FSU model but are parameterized in a postprocessing step. To account for possible errors in this parameterization step, we reduce the convective mass fluxes used in this analysis by 25% compared to those used by *Staudt et al.* [2001] and *Singh et al.* [2001]. This correction improves the simulation of HNO_3 as discussed in section 5. Dry deposition is as described by *Bey et al.* [2001a]. Nitric acid and H_2O_2 are scavenged by liquid and solid precipitation in convective updrafts and in large-scale systems as described by *Liu et al.* [2001]. This includes a scavenging efficiency of 40% km^{-1} in wet convective updrafts, which we reduce here to 20% km^{-1} for temperatures less than −15°C. There is substantial uncertainty regarding the uptake of HNO_3 by ice, with some studies indicating quantitative uptake [*Zondlo et al.*, 1997; *Abbatt*, 1997] and others suggesting column scavenging efficiencies of 10% or less [*Tabazadeh et al.*, 1999; *Meilinger et al.*, 1999; *Clegg and Abbatt*, 2001]. We discuss the sensitivity of the model results to the assumed scavenging efficiencies in section 5.

[16] Chemical perturbation to the NO_x budget from dust aerosols is also an important consideration for our simulation. Maximum export of desert dust from Asia occurs during spring [*Ginoux et al.*, 2001] and possibly impacts tropospheric chemistry over the North Pacific [*Dentener et al.*, 1996; *Tabazadeh et al.*, 1998; *He and Carmichael*, 1999; *Zhang and Carmichael*, 1999; *Martin et al.*, 2002]. We have implemented radiative and chemical effects of dust in the model as described by *Martin et al.* [2002] using monthly mean fields of mineral dust from *Ginoux et al.* [2001]. Partitioning of HNO_3 between gas and aerosol phases is not resolved in the model, and it is assumed for chemical reactivity purposes that HNO_3 is in the gas phase.

Table 1. Reactive Nitrogen Species Concentrations in the Tropical Pacific Troposphere[a]

Species	Upper Troposphere (6–12 km)		Lower Troposphere (0–6 km)	
	PEM-Tropics A	PEM-Tropics B	PEM-Tropics A	PEM-Tropics B
Tropical South Pacific (10°–30°S, 165°E–100°W)				
NO, pptv	37 (23–97)	25 (11–37)	8.8 (2.2–16)	2.0 (0.9–4.7)
NO_x,[b] pptv	61 (31–132)	33 (19–43)	23 (5.9–42)	7.9 (5.9–10)
HNO_3, pptv	103 (64–153)	37 (17–48)	126 (47–240)	36 (30–48)
HNO_3/NO_x, mol/mol	1.8 (1.1–3.2)	0.6 (0.5–1.3)	6.6 (3.1–9.9)	6.4 (4.6–8.3)
PAN, pptv	66 (47–116)	16 (12–24)	31 (2.6–132)	8.4 (2.0–26)
O_3, ppbv	49 (46–59)	24 (20–28)	53 (36–65)	17 (15–21)
Equatorial Pacific (10°S–10°N, 165°E–100°W)				
NO, pptv	18 (13–31)	16 (11–29)	1.8 (1.5–2.1)	4.1 (2.0–7.6)
NO_x,[b] pptv	28 (20–43)	24 (16–35)	4.1 (3.5–5.1)	8.2 (5.2–13)
HNO_3, pptv	66 (62–82)	41 (27–53)	45 (14–56)	28 (20–40)
HNO_3/NO_x, mol/mol	2.7 (1.3–4.0)	2.2 (0.6–2.6)	7.9 (3.7–10.6)	3.2 (2.2–5.2)
PAN, pptv	28 (21–33)	19 (13–29)	1 (1–1)	10 (1.9–33)
O_3, ppbv	34 (30–41)	25 (21–30)	11.4 (10.7–16)	9 (6–14)

[a]Median and interquartiles (values in parentheses) observed for 28 August to 6 October 1996 (PEM-Tropics A) and 1 March to 19 April 1999 (PEM-Tropics B). The observations have been averaged over the HNO_3 measurement interval.

[b]The sum of observed NO and modeled NO_2 for PEM-Tropics A and of observed NO and NO_2 for PEM-Tropics B.

Sequestration of HNO_3 in the aerosols could affect the NO_x budget if the gas-phase conversion rate of HNO_3 to NO_x differs largely from the parallel process involving aerosol nitrate, but the related aerosol chemistry is highly uncertain [*Jacob*, 2000].

[17] The model simulates 120 species to describe tropospheric O_3-NO_x-hydrocarbon chemistry, including 24 chemical tracers transported in the model. The chemical mechanism is that of *Horowitz et al.* [1998] with minor updates as discussed by *Bey et al.* [2001a], and is integrated with a fast Gear solver [*Jacobson and Turco*, 1994]. The rate of the $CH_3O_2 + HO_2$ reaction has been increased here by a factor of 3 at low temperature (220 K) relative to the standard recommendation [*DeMore et al.*, 1997], following the analysis of the HO_x budget in PEM-Tropics B by *Ravetta et al.* [2001]. Heterogeneous reactions involving aerosols use reaction probabilities from *Jacob* [2000] with sulfate aerosol fields from *Chin et al.* [1996] and dust aerosol fields as described above. Photolysis rates are computed with the fast J radiative transfer code of *Wild et al.* [2000], including Mie scattering by clouds with vertically resolved cloud optical depths from the FSU meteorological fields.

[18] Emissions of CO, NO_x, and hydrocarbons from fossil fuel combustion and industry are those described by *Wang et al.* [1998] for 1985 and are scaled to 1995 levels, the most recent year for which national emission estimates could be obtained, as described by *Bey et al.* [2001a]. Emissions of NO_x from lightning are parameterized from the FSU cloud top data following *Price and Rind* [1992] and *Pickering et al.* [1998] and are adjusted to yield a global source of 6 Tg N yr^{-1}, consistent with the *Martin et al.* [2002] model analysis of tropical tropospheric ozone. The sensitivity of results to the magnitude of the lightning source will be examined. Isoprene is emitted from terrestrial vegetation using the *Guenther et al.* [1995] scheme. Sources of acetone and CH_3CHO are as described by *Wang et al.* [1998] and include oxidation of hydrocarbons and emissions from biomass burning and biofuels. Acetone is also emitted by vegetation and industry. A minimum acetone concentration of 400 pptv is assumed, based on the PEM-Tropics B observations of *Singh et al.* [2001] and presumably reflecting an oceanic source [*Jacob et al.*, 2002]. Other biogenic emissions of organic species are assumed to play little photochemical role but are included as sources of CO [*Duncan et al.*, 2003].

[19] A particularly important issue for our simulation is the representation of biofuel use and biomass burning in Asia. We have implemented here a new inventory for emissions of CO from biofuel use with $1° \times 1°$ spatial resolution from *Yevich and Logan* [2003]. We have also included biofuel emissions of NO_x and hydrocarbons using emission factors from *Andreae and Merlet* [2001]. Biomass burning emissions for the PEM-Tropics B period are specified using fire count observations from the Along Track Scanning Radiometer-2 (ATSR-2) satellite [*Arino and Rosaz*, 1999] to scale a climatological inventory of biomass burned from R. M. Yevich and J. A. Logan (personal communication, 2001) to 1999 levels [*Duncan et al.*, 2003]. We apply emission factors (Table 2) for different vegetation types mostly following the recommendations of *Andreae and Merlet* [2001] to obtain emissions for CO, NO_x, and hydrocarbons.

[20] The distributions of NO_x emissions in the model from lightning, fossil fuel, biofuel, and biomass burning are shown in Figure 5, and regional emission totals for these different sources are summarized in Table 3. The largest NO_x source is from fossil fuel burning with comparable contributions from North America, Europe, and Asia. The lightning source is concentrated over continents in the Southern Hemisphere and over Indonesia, but there is also some activity over the South Pacific. Maximum biomass and biofuel burning emissions are from Southeast Asia and the Indian subcontinent.

[21] The fluxes from the stratosphere of O_3, NO_x, and HNO_3 contribute to the budgets of these species in the troposphere. The FSU model does not have the vertical resolution needed for an accurate simulation of stratospheric dynamics. We therefore use a cross-tropopause flux boundary condition for O_3 at 100 hPa altitude as described by *Wang et al.* [1998] with an annual global flux of 400 Tg yr^{-1} distributed by latitude and month of the year. We also

Table 2. Biomass Burning Emission Factors[a]

	NO	CO	C_2H_6	Acetone	C_3H_8	CH_2O	C_3H_6	Lumped Ketones[b]	Lumped Aldehydes[c]	Lumped Alkanes[d]
Savanna/grassland										
Global	3.9	65	0.32	0.44	0.09	0.35	0.48	0.52	0.38	0.015
North Africa[e]	1.1	-	-	-	-	-	-	-	-	-
Deforestation										
Tropical	1.6	100	0.5	0.62	0.15	1.4	0.99	0.84	0.59	0.24
Extratropical	3.0	97	0.6	0.56	0.25	2.2	1.0	0.90	0.67	0.32
Boreal[f]	0.44	120	-	-	-	-	-	-	-	-
Shrub fires										
Global	1.5	62	0.45	0.68	0.13	0.60	0.73	0.079	1.1	NA
Agriculture residue										
Global	2.5	92	0.97	0.63	0.52	1.4	1.2	0.82	0.54	0.27

[a]Units of g emitted gas/Tg dry matter burned.
[b]Lumped $\geq C_4$ ketones.
[c]Lumped $\geq C_3$ aldehydes.
[d]Lumped $\geq C_4$ alkanes.
[e]The global emission factors for savanna/grassland are used for North Africa except for NO.
[f]The global emission factors for deforestation are used for boreal forests except for NO and CO.

use a flux of 0.48 Tg N yr^{-1} of NO_y computed by *Wang et al.* [1998] which is transported across the tropopause as NO_x and HNO_3 with a molar ratio of 1:4.

[22] Simulations are conducted for a 3-month period from 22 January to 19 April 1999. The model is initialized on 21 January with mean January concentrations from the full-year CTM simulation of *Wang et al.* [1998] using general circulation model meteorology. Simulation through 1 March provides initialization of the transport patterns in the model, and we focus our attention on the 1 March to 19 April period.

4. Evaluation of Standard Simulation

[23] The CO concentrations produced by the model were discussed by *Staudt et al.* [2001] and found to reproduce the major vertical, latitudinal, and zonal gradients in the observations with no significant biases. In particular, the model reproduces the decreasing concentrations of CO with altitude in the Northern Hemisphere, the increasing concentrations with altitude in the Southern Hemisphere, and the longitudinal gradients above the equatorial Pacific driven by interhemispheric transport. Enhanced concentrations were observed and simulated in the lower troposphere above the western equatorial Pacific, where the river of pollution brought effluents from northern midlatitudes southward to about 10°S. In the upper troposphere, relatively high concentrations were found above the eastern equatorial Pacific, where northern hemispheric air was carried southward through a region of equatorial northwesterlies and into the general circulation of the Southern Hemisphere.

[24] The model simulation of oxygenated organic species, including formaldehyde (HCHO), PAN, acetone, and CH_3CHO was presented by *Singh et al.* [2001]. The model reproduces the vertical profile of HCHO well, with maximum underestimates of 40% above 9 km. The simulation of PAN, which will be discussed in more detail below, overestimates observations above the northern tropical Pacific and underestimates observations above the southern tropical Pacific. Simulated acetone concentrations as presented by *Singh et al.* [2001] were much lower than observed, and the imposition here of a minimum concentration of 400 pptv provides an ad hoc correction. A more thorough investigation of acetone sources and sinks using the PEM-Tropics B observations is presented by *Jacob et al.* [2002].

[25] Acetaldehyde concentrations over the South Pacific are underestimated by the model; simulated concentrations are 1–30 pptv, while the observations are 50–120 pptv and have little vertical gradient [*Singh et al.*, 2001]. No such underestimate is found when comparing model results with observations at continental sites (0.1–1 ppbv) [*Granby et al.*, 1997; *Riemer et al.*, 1998; *Christensen et al.*, 2000]. With a lifetime of about 1 day due to reaction with OH and photolysis, long-range transport of CH_3CHO from continental source regions to the remote Pacific troposphere is minimal. *Singh et al.* [2001] suggest that oxidation of nonmethane hydrocarbons not currently included in the model or photochemical degradation of organic material present in surface oceans may provide additional sources for CH_3CHO. However, imposing CH_3CHO concentrations in the model at the levels observed by *Singh et al.* [2001] would lead to severe discrepancies in the simulation of PAN and NO_x, as discussed in section 6.

[26] Figure 6 shows comparisons of model results (sampled along the flight tracks and for the flight days) with observed concentrations of O_3, OH, HO_2, NO, HNO_3, and PAN, as well as HNO_3/NO_x and PAN/NO_x concentration ratios, as a function of altitude and latitude. The model is largely successful at reproducing the observations over the tropical South Pacific. The low observed concentrations of O_3, NO, HNO_3, and PAN are well simulated south of 10°N. Rates of O_3 production and loss are similar to those obtained by *Olson et al.* [2001] with a photochemical point model constrained by local PEM-Tropics B observations.

[27] The model is less successful at reproducing the observations north of 10°N, where O_3 is overestimated by about 50%, NO by as much as a factor of 2, and HNO_3 and PAN by a factor of 2–5. We think that the model over-

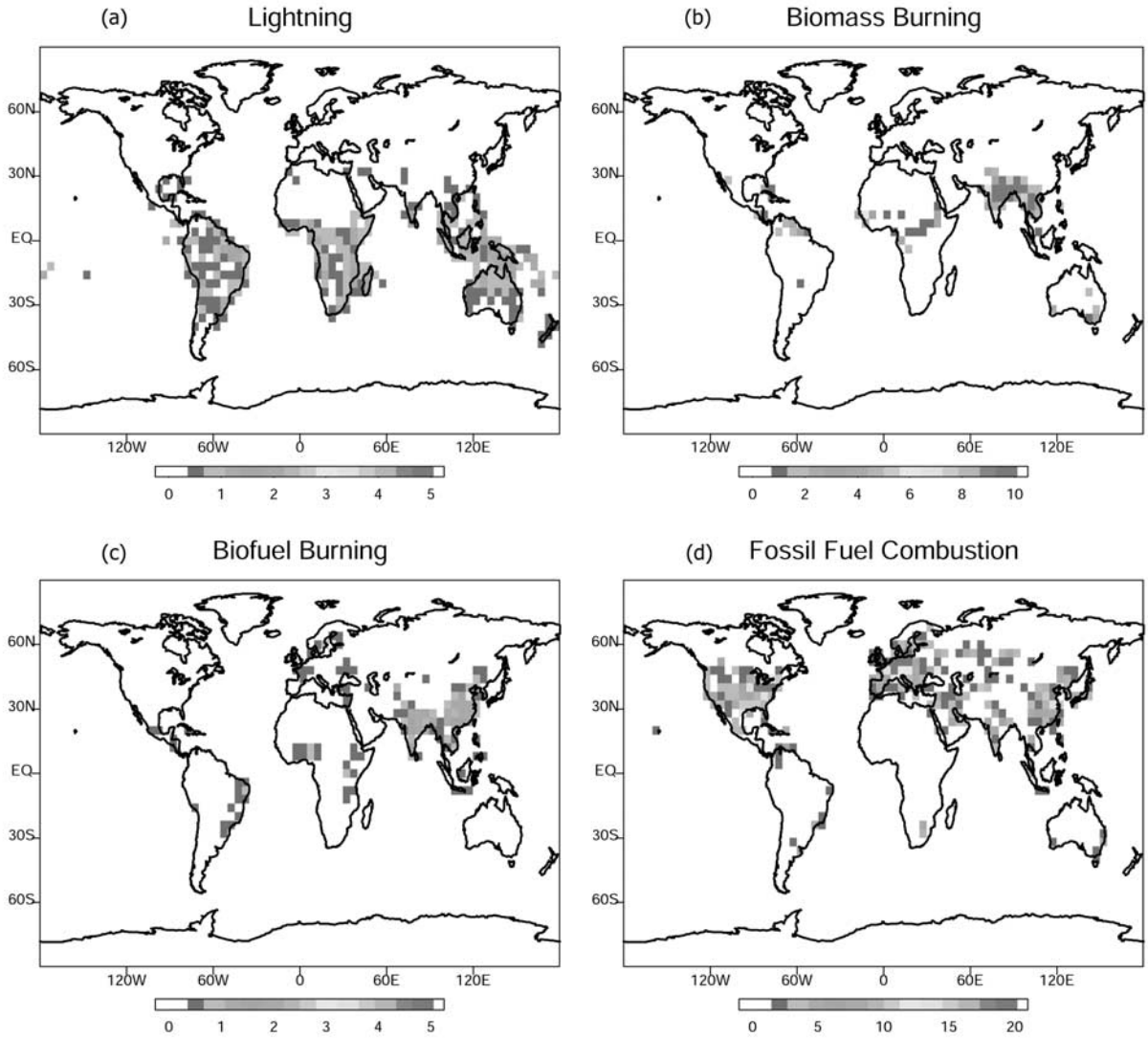

Figure 5. Distribution of NO_x emissions (units) used in the model for (a) lightning, (b) biomass burning, (c) biofuel burning, and (d) fossil fuel combustion. Values are averages for the PEM-Tropics B time period (1 March to 19 April 1999). See color version of this figure at back of this issue.

estimates over the North Pacific are caused by excessive vertical mixing at high latitudes in the model which brings air from the upper troposphere into the lower tropospheric flow around the North Pacific High. This dynamical problem in the model will affect species that have large vertical gradients in the far northern latitudes, including O_3, HNO_3, and PAN. The dynamically induced errors in these species in turn cause overestimates when they react above the tropical North Pacific. For example, high O_3 is responsible for OH overestimates near the surface north of the equator

Table 3. Global Emissions of NO_x for 1 March to 19 April 1999[a]

	North and Central America	Europe and Northern Africa	Asia and Indonesia	Southern Hemisphere	Total
Fossil fuel	0.90	0.95	0.83	0.20	2.88
Biofuel	0.012	0.07	0.16	0.05	0.29
Biomass burning	0.09	0.11	1.21	0.07	1.48
Soil	0.07	0.14	0.07	0.15	0.43
Lightning	0.05	0.09	0.08	0.43	0.65
Aircraft	0.03	0.02	0.01	0.01	0.07
Total	1.15	1.38	2.36	0.91	5.80

[a]Units of Tg N.

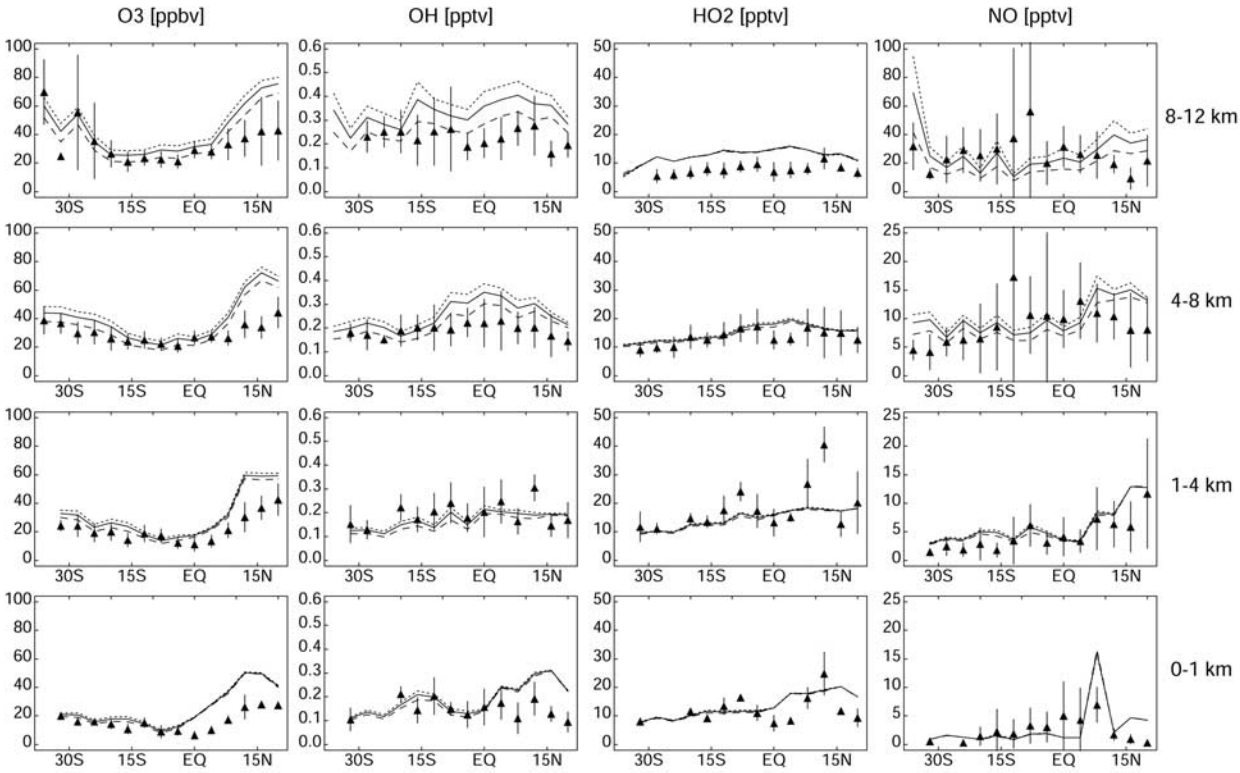

Figure 6. Latitudinal gradients of concentrations and concentration ratios over the Pacific in four altitude ranges from 0 to 12 km. Data for O_3, HNO_3, PAN, HNO_3/NO_x, and PAN/NO_x are 24-hour averages. Data for NO, OH, and HO_2 are mean daytime values (0900–1500 LT). Model results (lines) are compared to the PEM-Tropics B observations (solid triangles). The observations are averaged over 1 March to 19 April 1999, 150°E–90°W longitude, the specified altitude ranges, and 4° latitude bins. Vertical bars indicate standard deviations. The open triangles in the HNO_3 panel are total nitrate concentrations estimated from the mean observations of $HNO_3(g)$ in each latitudinal bin scaled by the corresponding mean observed ratio of $(HNO_3(g) + NO_3)/HNO_3(g)$ (Figure 3); since this scaling is based on aerosol NO_3^- concentrations above the detection limit, the resulting total nitrate concentrations are upper limits. All model results are sampled along the flight tracks and for the flight days, and the results are averaged across the same longitude and altitude ranges as the observations. The solid black line is for the standard simulation. The dotted gray line is for a simulation with emissions of NO_x from lightning increased by 50%. The dashed gray line for a simulation with NO_x emissions from lightning decreased by 50%.

and high HNO_3 and PAN cause NO to be too high at all altitudes north of about 10°N. The overestimate of O_3 above the North Pacific is largely insensitive to emissions from biomass burning, fossil fuel, and lightning. Likewise, we found that neither realistic variations in the initial conditions nor a zero flux boundary condition from the stratosphere provided much improvement in the simulation.

[28] The HO_x species (OH and HO_2) are well simulated in the lower troposphere, but are about 50% too high in the upper troposphere (Figure 6) with little dependence on latitude. Point photochemical model results of *Ravetta et al.* [2001] similarly overestimate OH and HO_2 observed above 8 km altitude during PEM-Tropics B, while other models overestimate HO_2 and underestimate OH [*Davis et al.*, 2001; *Tan et al.*, 2001; *Olson et al.*, 2001; J. M. Rodriguez et al., manuscript in preparation, 2001]. Increasing the rate of the $CH_3O_2 + HO_2$ reaction at low temperatures, as was done in our standard simulation following *Ravetta et al.* [2001] decreases OH and HO_2 concentrations in the upper troposphere by 4% and 10%, respectively.

[29] We find that mineral dust and sulfate aerosols exported from Asia across the North Pacific [*Ginoux et al.*, 2001; *Moore et al.*, 2003; *Clark et al.*, 2001] have only a modest effect on concentrations of NO, HNO_3, PAN, and O_3. Including mineral dust in the model decreases NO_x and PAN by up to 5 pptv in the middle and upper troposphere over the northeastern tropical Pacific, bringing the model into better agreement with the observations. Nitric acid in this region increases by 5–10 pptv because conversion from NO_x to HNO_3 is enhanced. The model HNO_3 is higher than the observations even after factoring in the contribution of NO_3^- observed in aerosols to the total observed HNO_3 (Figure 6). In the lower troposphere, NO_x, PAN, and HNO_3 decrease by 5–10 pptv when dust is added.

[30] The simulated concentrations of NO over the equatorial and southern Pacific (Figures 2 and 6) are generally within the range of the observed variability and reproduce the observed increase with altitude. The model underestimates NO in the equatorial marine boundary layer, where point photochemical model calculations constrained with

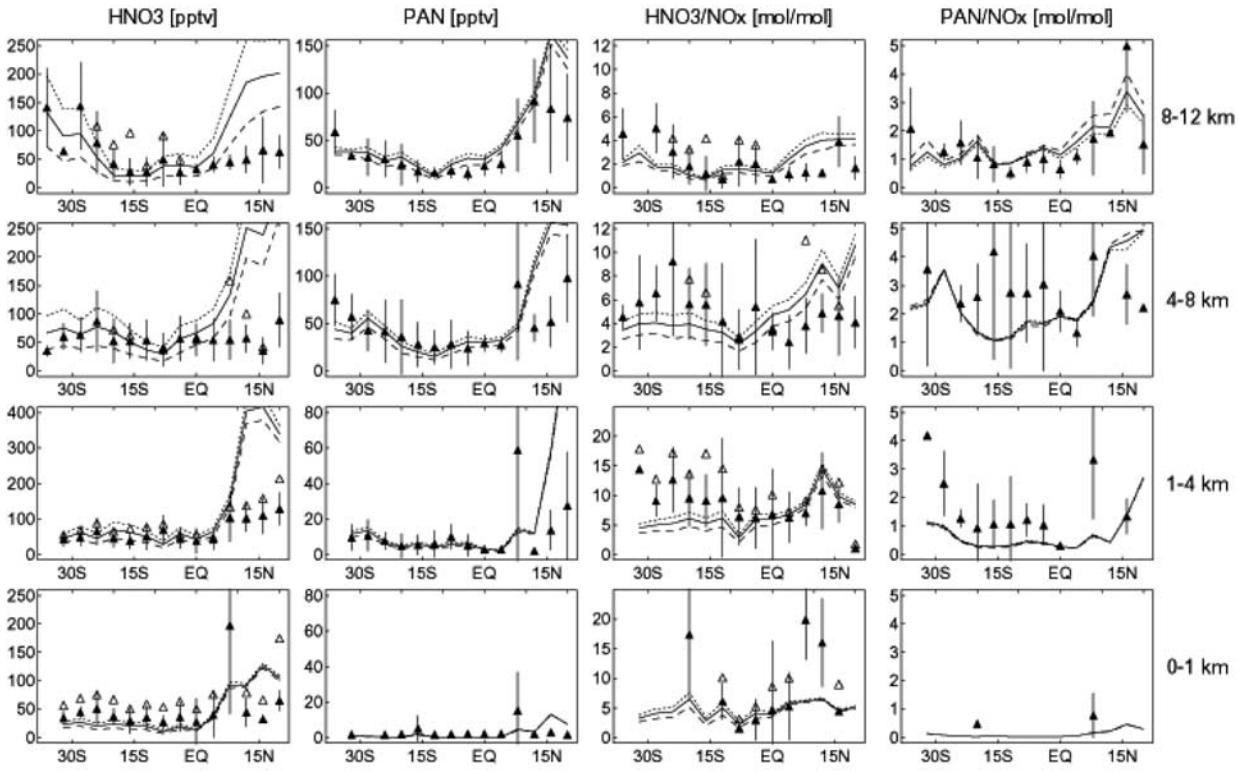

Figure 6. (continued)

the aircraft observations indicate that photolysis of methyl nitrate emitted from the ocean (not included in the 3-D model) can supply a few pptv NO_x. Simulated and observed concentrations of HNO_3 and PAN are minimum near the surface and in the equatorial upper troposphere where convection is active, resulting in midtropospheric maxima.

[31] The simulated concentration ratios for HNO_3/NO_x and PAN/NO_x generally capture observed concentrations (Figure 6). Discrepancies for HNO_3/NO_x are in the middle and upper troposphere south of 15°S, where the model is too low, and above 4 km altitude north of the equator, where the model is too high. Photochemical equilibrium models generally overestimate greatly the HNO_3/NO_x ratio in the remote troposphere, which has led to speculation about a missing chemical mechanism to convert HNO_3 to NO_x [*Chatfield*, 1994; *Hauglustaine et al.*, 1998; *Lary et al.*, 1997]. We find no support here for such a mechanism.

5. Sensitivity to Convective Mixing and Scavenging

[32] Concentrations of NO_y species (NO_x, HNO_3, and PAN) in the tropics are very sensitive to convection which provides an efficient sink through two pathways: (1) by bringing air rapidly down to the marine boundary layer where HNO_3 deposits to the surface and PAN thermally decomposes, and (2) by scavenging of HNO_3 via precipitation in the convective updrafts. If either of these processes is too strong in the model, then the simulated concentrations of HNO_3 and PAN and the simulated concentration ratio HNO_3/NO_x will be too low. We find that when scavenging of HNO_3 by ice in the model is allowed to proceed at the same rate as scavenging by liquid precipitation, HNO_3 above 6 km altitude is underestimated by 10–20 pptv over the South Pacific (Figure 7). Decreased scavenging of HNO_3 by ice improves the simulation over the South Pacific by increasing the concentrations of the NO_y species and the concentration ratio of HNO_3/NO_x throughout the column. When scavenging by ice is more rapid, HNO_3 concentrations are up to 50 pptv lower in the middle and upper troposphere over the North Pacific. Although the large overestimates of HNO_3 make it difficult to determine the appropriate level of scavenging, the large sensitivity of simulated HNO_3 to the scavenging parameterization points to a need to improve our understanding of the relative roles of ice and liquid scavenging. Indeed, adjusting the rate of scavenging by ice by 25% has a similar impact on the HNO_3 concentrations as decreasing the lightning source by 50% as discussed in section 7.

[33] We find in the standard version of the model (in which the convective mass fluxes are reduced by 25% from *Staudt et al.* [2001]) that the overturning of air in the 7.5–17 km altitude band over the South Pacific (2°N–30°S, 165°E–105°W) by convection-driven subsidence is 6% d^{-1}. The corresponding residence time of 15 days is consistent with other models of the tropical troposphere, providing support for the 25% reduction in convective mass fluxes. Using CH_3I observations, *Wang et al.* [2001] estimated a 10-day convective turnover timescale for the tropospheric column during PEM-Tropics B and a 20-day convective turnover timescale for PEM-Tropics A. *Prather and Jacob* [1997] derived a 20-day convective turnover

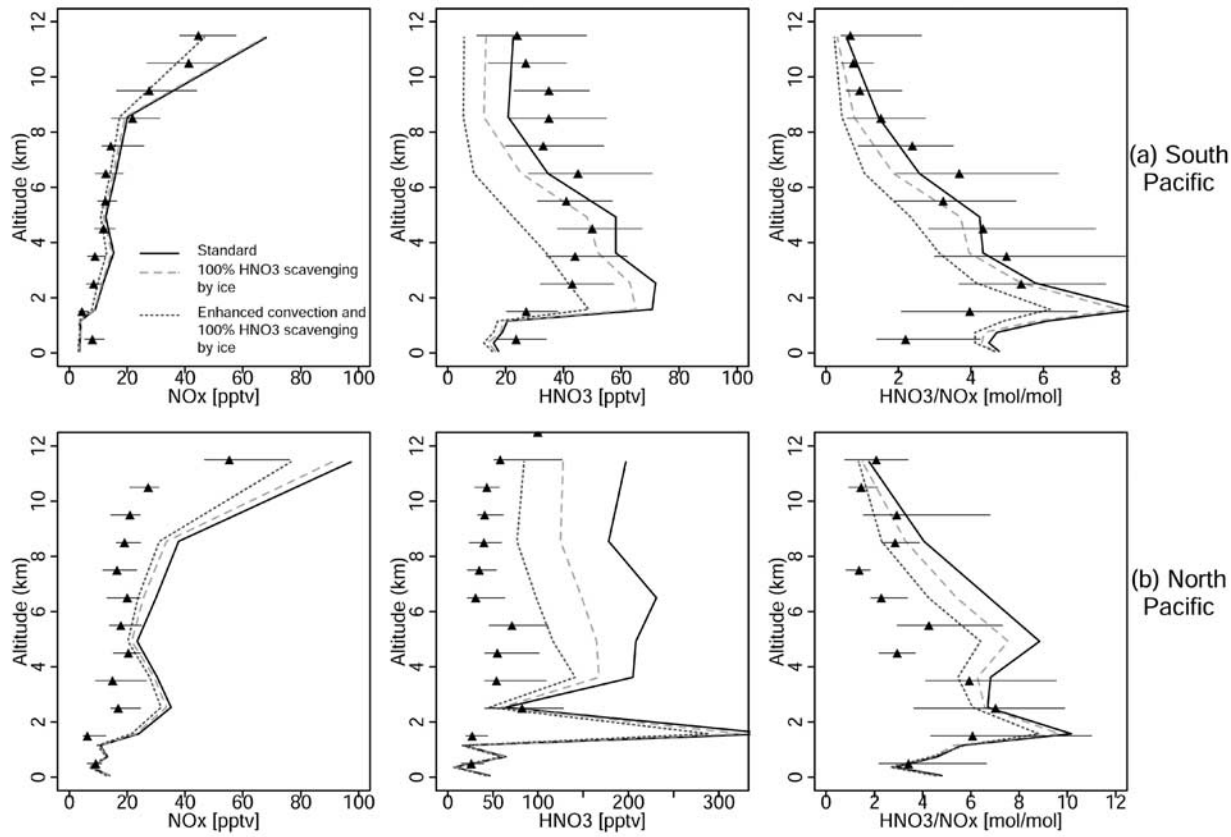

Figure 7. Vertical profiles of observed and simulated concentrations of NO_x and HNO_3, and HNO_3/NO_x concentration ratios over (a) the South Pacific (region a in Figure 1) and (b) the North Pacific (region b in Figure 1). The PEM-Tropics B observations (solid triangles) are averaged over 1 March to 19 April 1999, the area of each region, and 1-km altitude bins. Model results are averaged in the same way. Horizontal lines indicate minimum and maximum observations in each bin. Results from the standard simulation (solid line) are compared to results from sensitivity simulations with 100% scavenging of HNO_3 by ice (dashed line) and with both 100% scavenging of HNO_3 by ice and enhanced convection (dotted line).

timescale for 8–17 km altitude in the tropics using a general circulation model.

[34] In simulations where the rate of convective turnover is not reduced by 25%, simulated HNO_3 concentrations are depressed by 10–20 pptv throughout the tropospheric column over the South Pacific and up to 50 pptv over the North Pacific, causing a corresponding decrease in simulated HNO_3/NO_x (Figure 7). The concentration ratio of CH_3OOH/H_2O_2 (not shown) is another indicator of convection in the upper troposphere because CH_3OOH is elevated in convective outflow while H_2O_2 is depleted due to scavenging [*Cohan et al.*, 1999]. With more rapid convective turnover, CH_3OOH/H_2O_2 is overestimated by 25% over the South Pacific and by as much as a factor of 2 over the North Pacific.

6. Sensitivity to Oxygenated Organics

[35] Because the model does not include an oceanic source for acetone, it simulates acetone concentrations over the South Pacific (100–200 pptv) that are much lower than observed (400 pptv) [*Singh et al.*, 2001]. An ad hoc correction was applied in the standard simulation by imposing a minimum concentration of 400 pptv everywhere. When acetone is not constrained in this way, PAN and PAN/NO_x are underestimated over the South Pacific, as shown in Figure 8.

[36] Despite improvements achieved with fixed acetone, the model still underestimates the PAN/NO_x concentration ratio in the midtroposphere and near the surface over the South Pacific region. Because the majority of PAN measurements near the surface were below the 1 pptv detection limit, the mean observed PAN and PAN/NO_x shown in Figure 8 are too high. The model underestimate of PAN/NO_x in the midtroposphere, however, may indicate that simulated concentrations of the peroxy acetyl radical ($CH_3C(O)OO$) are too low there. As mentioned previously, the model substantially underestimates the PEM-Tropics B observations of CH_3CHO, an important PAN precursor, while producing concentrations in the continental boundary layer comparable to prior observations.

[37] To test the impact of higher levels of CH_3CHO on the NO_x chemistry, we conducted a sensitivity simulation in

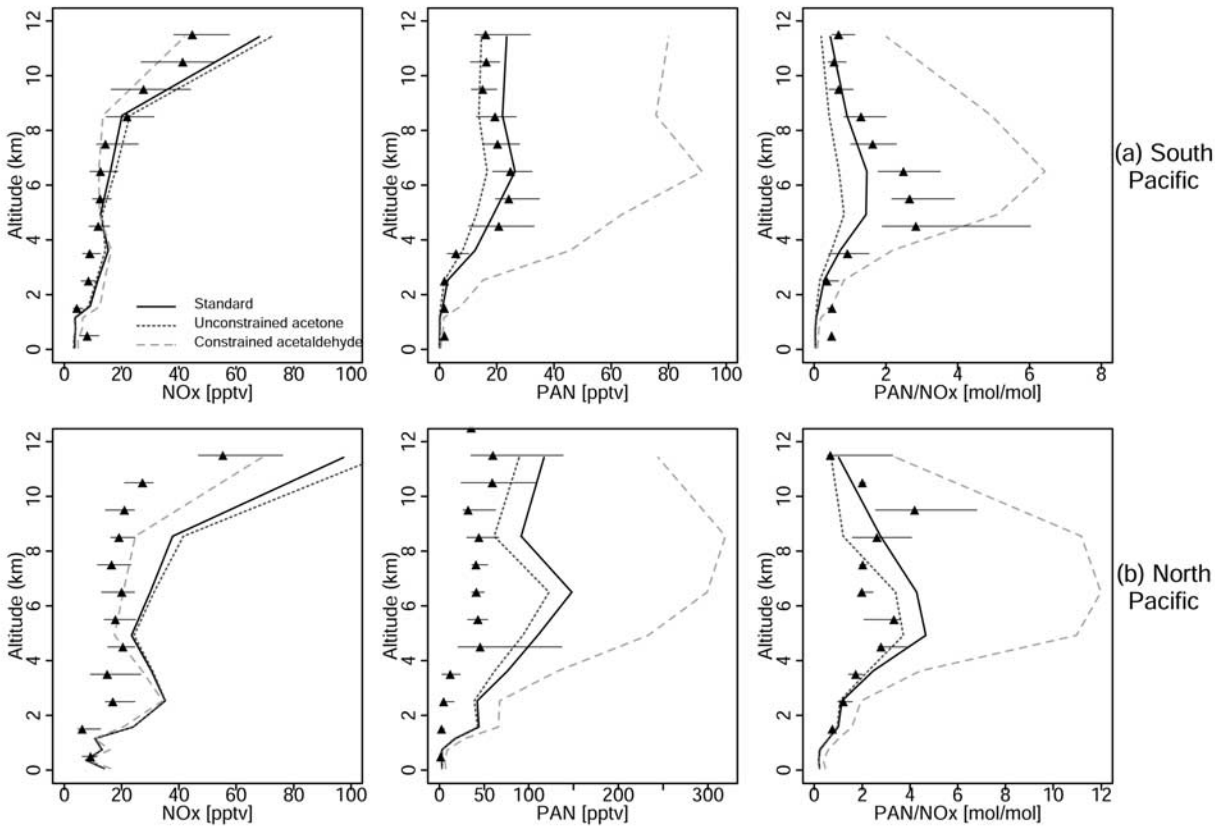

Figure 8. Vertical profiles of observed and simulated concentrations of NO_x and PAN, and PAN/NO_x concentration ratios, over (a) the South Pacific (region a in Figure 1) and (b) the North Pacific (region b in Figure 1). The PEM-Tropics B observations (solid triangles) are averaged over 1 March to 19 April 1999, the area of each region, and 1- km altitude bins. Horizontal lines indicate minimum and maximum observations in each bin. Model results are averaged in the same way. The standard simulation (solid line), a simulation without acetone constrained to the 400 pptv minimum (dotted line), and a simulation without CH_3CHO constrained to an 80 pptv minimum (dashed line) are shown.

which CH_3CHO was set to a minimum concentration of 80 pptv to match the PEM-Tropics B observations of *Singh et al.* [2001] without perturbing the simulated distribution over continents where no bias with observations is apparent. When CH_3CHO concentrations are constrained, the simulated PAN concentrations and PAN/NO_x concentration ratios are 2–6 times higher than observed in the middle and upper troposphere, while still underestimating PAN/NO_x near the surface (Figure 8). In addition, the HNO_3/NO_x ratio in the lower troposphere is decreased by up to a factor of 2 reflecting the enhanced release of NO_x from PAN transported into the region. These large discrepancies between observed and simulated PAN indicate that our current understanding of NO_y chemical cycling appears to be incompatible with the free tropospheric observations of CH_3CHO during PEM-Tropics B. Only near the surface does increased CH_3CHO appear consistent with the NO_x and HO_x chemistry, suggesting an oceanic source may be present.

7. Constraining the Lightning NO_x Source

[38] Considerable uncertainty is associated with the magnitude, location, vertical distribution, and timing of NO_x emissions from lightning. We conducted two simulations with lightning emissions reduced by 50% to 3 Tg N yr^{-1} (dashed lines in Figure 6) and increased by 50% to 9 Tg N yr^{-1} (dotted lines) to see if the PEM-Tropics B observations could be used to constrain the magnitude of this source. Since the lightning source is located primarily over tropical continents, the changes in concentrations simulated over the tropical Pacific reflect the impact of aged emissions. Decreasing lightning improves the simulation of upper tropospheric OH and of upper tropospheric HNO_3 in the Northern Hemisphere. On the other hand, increasing lightning improves the simulation of HNO_3 in the upper troposphere south of 20°S, while exacerbating the HNO_3 overestimate above the North Pacific. Other species are not much impacted by changing the lightning NO_x emissions.

[39] Lightning emissions have a rather small effect on HNO_3/NO_x. Increasing lightning reduces the discrepancy between model and observed HNO_3/NO_x over the South Pacific, but aggravates model overestimates over the North Pacific. We find that increasing the lightning source actually causes a slight increase in the simulated HNO_3/NO_x above the tropical Pacific, contrary to what might have been

expected. The additional NO_x from lightning increases OH (Figure 6), which shortens the NO_x lifetime. The HNO_3/NO_x ratio is more sensitive to the rate of convective overturning and associated scavenging than to the source of NO_x from lightning (see section 5).

[40] The fact that increased emission of NO_x from lightning improves the simulation above the tropical South Pacific while degrading the simulation above the tropical North Pacific might suggest a model error in the distribution of lightning emissions. However, we find that the geographic distribution (Figure 5) is consistent with satellite observations. Observations of lightning strikes from the satellite-based Lightning Imaging Sensor (LIS) indicate maximum lightning in the southern tropics during March and a northward shift during April [*Fuelberg et al.*, 2001]. Using observations from the satellite-based Optical Transient Detector (OTD) to derive NO_x emissions from lightning, *Nesbitt et al.* [2000] similarly find maximum emissions over the southern tropics during December–January–February, shifting to a maximum extending from 10°S to 40°N during March–April–May. Maximum emissions of NO_x from lightning in our model for 1 March 1999 to 15 April 1999 are likewise found between 20°S and 10°N.

8. NO_x Budget for the Tropical Pacific Troposphere

[41] Primary sources for NO_x in the Southern Hemisphere during the PEM-Tropics B period are dominated by lightning followed by fossil fuel combustion and soils (Table 3). The impact of these sources on concentrations of NO_x simulated over the tropical South Pacific (region a in Figure 1) is illustrated in Figure 9 using results from sensitivity simulations with individual sources shut off. At 8–12 km altitude, shutting lightning off reduces NO_x concentrations over the tropical South Pacific by 76%, while HNO_3 and PAN (not shown) decrease by 86% and 65%, respectively. Ozone and OH likewise show reductions in the upper troposphere of 48% and 45%, respectively, when lightning is turned off. Lightning remains the largest primary source for NO_x, HNO_3, and PAN at 2–8 km altitude. Near the surface, fossil fuel makes a larger contribution to simulated NO_x and HNO_3 concentrations, although lightning still accounts for about half of the simulated HNO_3.

[42] The primary sources of NO_x in the Northern Hemisphere during PEM-Tropics B are estimated to be a factor of 5 greater than those in the Southern Hemisphere (Table 3). Anthropogenic emissions from fossil fuel, biofuel, and aircraft contribute 68% of the northern hemispheric source, while lightning contributes only 5%. Nevertheless, as illustrated in Figure 9, lightning is the most important source of NO_x in the upper troposphere over the northern tropical Pacific. Concentrations of HNO_3 and, to a lesser extent, PAN are also enhanced by NO_x emissions from lightning (not shown). This result is robust because the excessive transport from the high northern latitudes would tend amplify the influence of Northern Hemispheric sources. Concentrations of PAN in the upper and midtroposphere are more sensitive to biomass burning emissions, which only affect NO_x and HNO_3 in the 2–8 km altitude range. Below 4 km, the influence of fossil fuel emissions is dominant (Figure 9), consistent with past studies that found boundary layer air observed above the North Pacific during PEM-Tropics B to have strong Asian and European pollution influence due to circulation around the Pacific High and into the trade winds [*Moxim et al.*, 1996; *Blake et al.*, 2001; *Staudt et al.*, 2001]. We find here that this pollution influence extends to NO_x.

[43] The NO_x budget above the South Pacific is given in Table 4 for the standard simulation. The model limitations over the North Pacific and the smaller area spanned by the aircraft make it imprudent to consider the budget of that region. For the tropical South Pacific, the NO_x source to the lower troposphere is mostly from decomposition of PAN (74%), with secondary contributions from decomposition of HNO_3 (11%) and transport of NO_x into the region (11%). The chemical sources and sinks of NO_x in the lower troposphere are close to steady state because the budget is dominated by cycling with HNO_3 and PAN.

[44] The NO_x sources to the upper troposphere above the South Pacific are more distributed, with contributions from transport into the region (34%), emissions from lightning (19%), and chemical recycling from HNO_3 (23%) and PAN (23%). The chemical imbalance in the upper troposphere, diagnosed by the ratio of NO_x chemical losses (LNO_x) to NO_x chemical sources (PNO_x) in the 3-D model, is equal to 2.0, compared to an imbalance of 1.6 computed in the 3-D model for the PEM-Tropics A time period [*Staudt et al.*, 2002]. The larger chemical imbalance during PEM-Tropics B is confirmed by a lower HNO_3/NO_x concentration ratio in the observations (Table 1) and the model (1.9 for PEM-Tropics A, 1.5 for PEM-Tropics B). Similar to PEM-Tropics A, the imbalance during PEM-Tropics B is largely maintained by the input of fresh NO_x from lightning into the upper troposphere, where the NO_x lifetime is about 10 days. Turning off the source of NO_x from lightning reduces LNO_x/PNO_x from 2.0 to 1.3. For the same region during PEM-Tropics A, *Staudt et al.* [2002] found that recycling of HNO_3 and PAN contributed 63% of the NO_x source. Chemical recycling was more important during PEM-Tropics A because the NO_x source from biomass burning, which had aged 1–2 weeks by the time it reached the Pacific, was much larger while the NO_x source from in situ lightning emissions was a factor of 2 less. In addition, more rapid convective overturning during PEM-Tropics B [*Wang et al.*, 2001] created a larger chemical imbalance in the NO_x budget by enhancing HNO_3 loss.

9. Summary

[45] We examined the sources and chemistry affecting NO_x over the tropical Pacific during the PEM-Tropics B aircraft campaign March–April 1999 by using a global 3-D model of tropospheric chemistry driven by assimilated meteorological data. The model reproduces the particularly low concentrations of NO (1–5 pptv), HNO_3 (20–50 pptv), and PAN (<1–10 pptv) observed in the lower troposphere above the equatorial and southern Pacific. Low concentrations of HNO_3 (10–50 pptv) and PAN (10–30 pptv) observed in the upper equatorial troposphere, because of convection linking it to the lower troposphere, are also reproduced by the model, resulting in midtroposphere maxima for these species. Simulated and observed NO concentrations are maximum in the upper troposphere

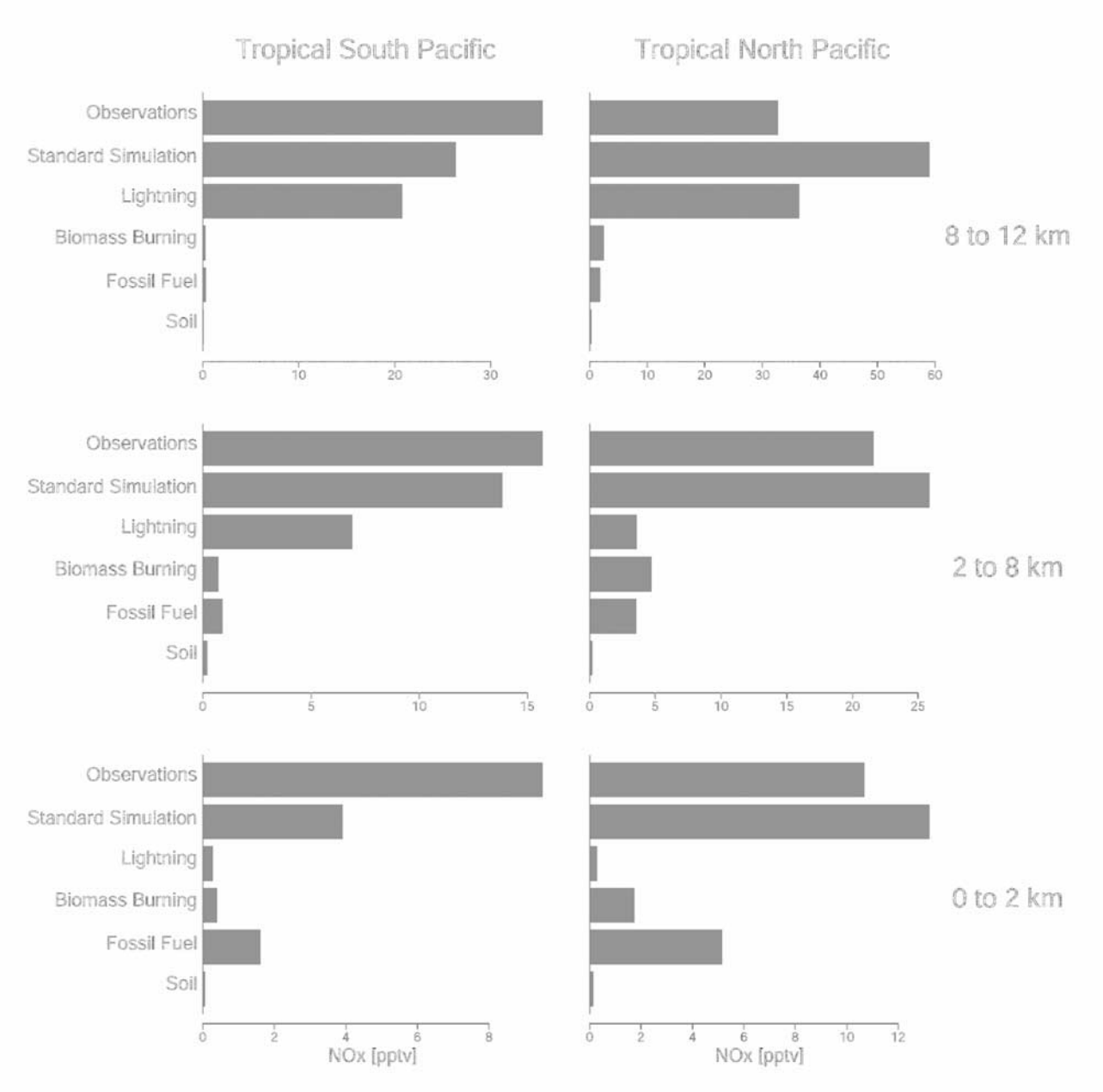

Figure 9. Bar plots showing the average observed and simulated concentrations of NO_x for three altitude ranges over (left) the tropical South Pacific and (right) the tropical North Pacific. Results are shown for the standard simulation and for the differences between the standard simulation and a series of simulations with no emissions from lightning, from biomass burning, from fossil fuel combustion, and from soils or fertilizer.

(10–100 pptv), due to emissions from lightning. The model is less successful over the North Pacific, where excessive vertical mixing in the high latitudes brings air with elevated O_3, HNO_3, and PAN into the lower tropospheric flow around the North Pacific High.

[46] Concentrations of NO, HNO_3, and PAN observed during PEM-Tropics B are generally lower than those observed over the South Pacific during PEM-Tropics A over the same region but in September–October 1996. PEM-Tropics A was conducted in the biomass burning season of the southern tropics and long-range transport of combustion effluents elevated NO_x, HNO_3, and PAN concentrations throughout the South Pacific atmosphere. PEM-Tropics B was conducted in the wet season of the southern tropics but the biomass burning season of the northern tropics, and this combustion influence was observed over the North Pacific superimposed to that from fossil fuel combustion.

[47] Lightning was the dominant source of NO, HNO_3, and PAN above the equatorial and southern Pacific during PEM-Tropics B. Turning off the source of NO_x from lightning in the model decreases the NO_x source to the region by a factor of 7 in the upper troposphere and a factor of 3 in the lower troposphere. Lightning contributed most of the NO_x

Table 4. NO_x Budget for the Southern Tropical Pacific Troposphere[a]

Process	Lower Troposphere 0–6 km	Upper Troposphere 6–12 km
Sources, Mmol d^{-1}		
Net transport into region	12.8 (11%)	17.2 (34%)
Emissions (lightning + aircraft)	3.7 (3%)	9.6 (19%)
Chemical production (PNO_x)		
$HNO_3 \rightarrow NO_x$	12.5 (11%)	11.6 (23%)
$PAN \rightarrow NO_x$	86.3 (74%)	11.8 (23%)
alkyl nitrates[a] $\rightarrow NO_x$	1.8 (1%)	0.8 (1%)
Total	117	51.0
Sinks, Mmol d^{-1}		
Chemical loss (LNO_x)		
$NO_x \rightarrow HNO_3$	45.4 (40%)	32.2 (67%)
$NO_x \rightarrow PAN$	66.1 (59%)	15.5 (32%)
$NO_x \rightarrow$ alkyl nitrates[b]	1.2 (1%)	0.6 (1%)
Total	113	48.3
Accumulation, Mmol d^{-1}	4	1.8
NO_x lifetime, days	0.84	3.0
Chemical Imbalance (LNO_x/PNO_x):		
This model	1.1	2.0
Photochemical point model[c]	0.5	1.5

[a]Budget terms are model averages from the standard simulation for a region defined as 2°N–30°S and 165°E–100°W (an area of 3.4×10^{13} m^2) and for the PEM-Tropics B time period of 1 March to 19 April 1999. For the purposes of this budget, we use an expanded chemical family definition of NO_x ($NO_x = NO + NO_2 + NO_3 + HNO_2 + HNO_4 + 2*N_2O_5$).

[b]Includes the products of nonmethane hydrocarbon oxidation but no contribution from oceanic emissions.

[c]Photochemical point model calculation by *Ravetta et al.* [2001] for the ensemble of PEM-Tropics B flight tracks.

in the upper troposphere; lightning, biomass burning, and fossil fuels all made significant contributions in the middle troposphere, while fossil fuel combustion was the most important source of NO_x to the lower troposphere.

[48] We find that the simulation of HNO_3 and HNO_3/NO_x over the tropical Pacific is very sensitive to the rate of convective overturning and convective scavenging of HNO_3. The simulation of HNO_3 and HNO_3/NO_x is improved when the scavenging efficiency of HNO_3 by ice in the convective updrafts is less than that by liquid precipitation. Increasing the convective turnover rate by 25% causes HNO_3 to decrease by 10–20 pptv above the South Pacific and by up to 50 pptv above the North Pacific. The HNO_3/NO_x concentration ratio is lower when convection is more vigorous.

[49] PEM-Tropics B provided the first observations of oxygenated organics in the tropical marine atmosphere. Average concentrations observed for acetone (431 pptv) and CH_3CHO (78 pptv) were much higher than simulated by the model without an oceanic source. To account for such an oceanic source we constrained acetone in the standard simulation to a minimum value of 400 pptv, which provided an improved simulation of PAN and PAN/NO_x. When we also constrained CH_3CHO to a minimum value of 80 pptv, simulated PAN concentrations and PAN/NO_x concentration ratios were several times higher than observed. The high observed CH_3CHO concentrations above the South Pacific can not be reconciled with our understanding of PAN chemistry.

[50] During PEM-Tropics B, chemical losses of NO_x exceeded chemical sources by a factor of 2 at 6–12 km altitude above the equatorial and southern Pacific; a chemical imbalance also apparent in the observed HNO_3/NO_x ratios. Lightning emissions and convective overturning were the main causes for this chemical imbalance. There was no evidence for a missing chemical pathway recycling HNO_3 to NO_x. During PEM-Tropics A, NO_x chemical sinks exceeded chemical sources in the South Pacific upper troposphere by only 60%, and HNO_3/NO_x concentration ratios were correspondingly higher than in PEM-Tropics B, because the large biomass burning contribution was close to chemical steady state and convection was less active. Observed HNO_3 concentrations and HNO_3/NO_x concentration ratios in this region were a factor of 3 less during PEM-Tropics B than during PEM-Tropics A.

[51] **Acknowledgments.** This research was funded by the NASA Tropospheric Chemistry Program (TCP).

References

Abbatt, J. P., Interaction of HNO_3 with water-ice surfaces at temperatures of the free troposphere, *Geophys. Res. Lett.*, *24*, 1479–1482, 1997.

Andreae, M. O., and P. Merlet, Emission of trace gases and aerosols from biomass burning, *Global Biogeochem. Cycles*, *15*, 955–966, 2001.

Arino, O., and J.-M. Rosaz, 1997 and 1998 World ATSR Fire Atlas using ERS-2 ATSR-2 Data, in *Proceedings from the Joint Fire Science Conference and Workshop*, 7 pp., Joint Fire Sci. Program, Boise, Idaho, 1999.

Bey, I., D. J. Jacob, R. M. Yantosca, J. A. Logan, B. Field, A. M. Fiore, Q. Li, H. Liu, L. J. Mickley, and M. Schultz, Global modeling of tropospheric chemistry with assimilated meteorology: Model description and evaluation, *J. Geophys. Res.*, *106*, 23,073–23,095, 2001a.

Bey, I., D. J. Jacob, J. A. Logan, and R. M. Yantosca, Asian chemical outflow to the Pacific in spring: Origins, pathways, and budgets, *J. Geophys. Res.*, *106*, 23,097–23,113, 2001b.

Blake, N. J., et al., Large scale latitudinal and vertical distributions of NMHCs and selected halocarbons in the troposphere over the Pacific Ocean during the March–April 1999 Pacific Exploratory Expedition (PEM-Tropics B), *J. Geophys. Res.*, *106*, 32,627–32,644, 2001.

Bradshaw, J., et al., Photofragmentation two-photon laser-induced fluorescence detection of NO2 and NO: Comparison of measurements with model results based on airborne observations during PEM-Tropics A, *Geophys. Res. Lett.*, *26*, 471–474, 1999.

Chatfield, R. B., Anomalous HNO_3/NO_x ratio of remote tropospheric air: Conversion of nitric acid to formic acid and NO_x?, *Geophys. Res. Lett.*, *21*, 2705–2708, 1994.

Chin, M., D. J. Jacob, J. W. Munger, D. D. Parish, and B. G. Doddridge, Relationship of ozone and carbon monoxide over North America, *J. Geophys. Res.*, *101*, 2111–2134, 1996.

Christensen, C. S., H. Skov, T. Nielsen, and C. Lohse, Temporal variation of carbonyl compound concentrations at a semi-rural site in Denmark, *Atmos. Environ.*, *34*, 287–296, 2000.

Clark, A., W. Collins, P. Rasch, V. Kasputin, K. Moore, and S. Howel, Dust and pollution transport on global scales: Aerosol measurements and model predictions, *J. Geophys. Res.*, *106*, 32,555–32,556, 2001.

Clegg, S. M., and J. P. D. Abbatt, Uptake of gas-phase SO_2 and H_2O_2 by ice surfaces: Dependence on partial pressures, temperature and surface acidity, *J. Phys. Chem. A*, *105*, 6630, 2001.

Cohan, D. S., M. G. Schultz, D. J. Jacob, B. G. Heikes, and D. R. Blake, Convective injection and photochemical decay of peroxides in the tropical upper troposphere: Methyl iodide as a tracer of marine convection, *J. Geophys. Res.*, *104*, 5717–5724, 1999.

Davis, D., et al., Marine latitude/altitude OH distributions: Comparison of Pacific ocean observations with models, *J. Geophys. Res.*, *106*, 32,691–32,708, 2001.

DeMore, W. B., S. P. Sanders, D. M. Golden, R. G. Hamspon, M. J. Kurylo, C. J. Howard, A. R. Ravishankara, C. E. Kolb, and M. J. Molina, Chemical kinetic and photochemical data for use in stratospheric modeling, *JPL Publ. 97-4*, 1997.

Dentener, F. J., G. R. Carmichael, Y. Zhang, J. Lelieveld, and P. J. Crutzen, Role of mineral aerosol as a reactive surface in the global troposphere, *J. Geophys. Res.*, *101*, 22,869–22,889, 1996.

Dibb, J. E., R. W. Talbot, G. Seid, C. Jordan, E. Scheuer, E. Atlas, N. J. Blake, and D. R. Blake, Airborne sampling of aerosol particles: Comparison between surface sampling at Christmas Island and P-3 sampling during PEM-Tropics B, *J. Geophys. Res.*, *107*, 8230, doi:10.1029/2001JD000408, 2002. [printed *108*(D2), 2003]

Duncan, B., R. Martin, A. Staudt, R. Yevich, and J. Logan, Interannual and seasonal variability of biomass burning emissions constrained by satellite observations, *J. Geophys. Res.*, *108*, doi:10.1029/2002JD002378, in press, 2003.

Emmons, L., et al., Climatologies of NOx and NOy: A comparison of data and models, *Atmos. Environ.*, *31*, 1851–1904, 1997.

Fuelberg, H. E., R. E. Newell, D. J. Westberg, J. C. Maloney, J. R. Hannan, B. C. Martin, M. A. Avery, and Y. Zhu, A meteorological overview of the second Pacific Exploratory Mission in the Tropics, *J. Geophys. Res.*, *106*, 32,427–32,444, 2001.

Gairola, R. M., and T. N. Krishnamurti, Rain rates based on SSM/I, OLR and raingauge data sets, *Meteorol. Atmos. Phys.*, *50*, 165–174, 1992.

Ginoux, P., M. Chin, I. Tegen, J. Prospero, B. Holben, O. Dubovik, and S.-J. Lin, Sources and distributions of dust aerosols simulated with the GOCART model, *J. Geophys.Res.*, *106*, 20,255–20,274, 2001.

Granby, K., C. S. Christensen, and C. Lohse, Urban and semi-rural observations of carboxylic acids and carbonyls, *Atmos. Environ.*, *31*, 1403–1415, 1997.

Gregory, G. L., et al., Chemical characteristics of Pacific tropospheric air in the region of the ITCZ and SPCZ, *J. Geophys. Res.*, *104*, 5677–5696, 1999.

Guenther, A., et al., A global model of natural volatile organic compound emissions, *J. Geophys. Res.*, *100*, 8873–8892, 1995.

Hauglustaine, D. A., G. P. Brasseur, S. Walters, P. J. Rasch, J. F. Muller, L. K. Emmons, and M. A. Carroll, MOZART, a global chemical transport model for ozone and related chemical tracers, 2, Model results and evaluation, *J. Geophys. Res.*, *103*, 28,291–28,335, 1998.

He, S., and G. R. Carmichael, Sensitivity of photolysis rates and ozone production in the troposphere to aerosol properties, *J. Geophys. Res.*, *104*, 26,307–26,324, 1999.

Hoell, J. M., D. D. Davis, D. J. Jacob, M. O. Rodgers, R. E. Newell, H. E. Fuelberg, R. J. McNeal, J. L. Raper, and R. J. Bendura, Pacific Exploratory Mission in the tropical Pacific: PEM-Tropics A, August–September 1996, *J. Geophys. Res.*, *104*, 5567–5583, 1999.

Horowitz, L. W., J. Y. Liang, G. M. Gardner, and D. J. Jacob, Export of reactive nitrogen from North America during summertime, *J. Geophys. Res.*, *103*, 13,435–13,450, 1998.

Jacob, D. J., Heterogeneous chemistry and tropospheric ozone, *Atmos. Environ.*, *34*, 2131–2159, 2000.

Jacob, D. J., B. D. Field, E. M. Jin, I. Bey, Q. Li, J. A. Logan, R. M. Yantosca, and H. B. Singh, Atmospheric budget of acetone, *J. Geophys. Res.*, *107*(D10), 4100, doi:10.1029/2001JD000694, 2002.

Jacobson, M. Z., and R. P. Turco, SMVGEAR: A sparse-matrix, vectorized gear code for atmospheric models, *Atmos. Environ.*, *28*, 273–284, 1994.

Krishnamurti, T. N., S. Low-Nam, and T. Pasch, Cumulus parameterization and rainfall rates II, *Mon. Weather Rev.*, *111*, 815–828, 1983.

Krishnamurti, T. N., H. E. Fuelberg, M. C. Sinha, D. Oosterhof, E. L. Bensman, and V. B. Kumar, The meteorological environment of the tropospheric ozone maximum over the tropical South Atlantic, *J. Geophys. Res.*, *98*, 10,621–10,641, 1993.

Krishnamurti, T. N., M. C. Sinha, M. Kanamitsu, D. Oosterhof, H. Fuelberg, R. Chatfield, D. J. Jacob, and J. A. Logan, Passive tracer transport relevant to the TRACE-A experiment, *J. Geophys. Res.*, *101*, 23,889–23,907, 1996.

Lamarque, J.-F., G. P. Brasseur, P. G. Hess, and J.-F. Muller, Three-dimensional study of the relative contributions of the different nitrogen sources in the troposphere, *J. Geophys. Res.*, *101*, 22,955–22,968, 1996.

Lary, J., A. M. Lee, R. Toumi, M. J. Newchurch, M. Pirre, and J. B. Renard, Carbon aerosols and atmospheric photochemistry, *J. Geophys. Res.*, *102*, 3671–3682, 1997.

Lee, D. S., I. Kohler, E. Grobler, F. Rohrer, R. Sausen, L. Gallardo-Klenner, J. G. J. Olivier, F. J. Dentener, and A. F. Bouwman, Estimations of global NO_x emissions and their uncertainties, *Atmos. Environ.*, *31*, 1735–1749, 1997.

Levy, H., II, W. J. Moxim, A. A. Klonecki, and P. S. Kasibhatla, Simulated tropospheric NO_x: Its evaluation, global distribution and individual source contributions, *J. Geophys. Res.*, *104*, 26,279–26,306, 1999.

Liu, H., D. J. Jacob, I. Bey, and R. M. Yantosca, Constraints from 210Pb and 7Be on wet deposition and transport in a global three-dimensional chemical tracer model driven by assimilated meteorological fields, *J. Geophys. Res.*, *106*, 12,109–12,128, 2001.

Mari, C., et al., Sources of upper tropospheric HO_x over the South Pacific Convergence Zone: A case study, *J. Geophys. Res.*, doi:10.1029/2000JD000304, in press, 2003.

Martin, R. V., D. J. Jacob, J. A. Logan, I. Bey, R. M. Yantosca, A. C. Staudt, Q. Li, A. M. Fiore, B. N. Duncan, H. Liu, P. Ginoux, and V. Thouret, Interpretation of TOMS observations of tropical tropospheric ozone with a global model and in-situ observations, *J. Geophys. Res.*, *107*(D18), 4351, 10.1029/2001JD001480, 2002.

Meilinger, S. K., et al., HNO_3 partitioning in cirrus clouds, *Geophys. Res. Lett.*, *26*, 2207–2210, 1999.

Merrill, J. T., Atmospheric long-range transport to the Pacific Ocean, in *Chemical Oceanography*, vol. 10, edited by R. A. Duce, J. P. Riley, and R. Chester, pp. 15–50, Academic, San Diego, Calif., 1989.

Moore, K., A. D. Clarke, V. Kapustin, and S. Howell, Long range transport of continental plumes over the Pacific Basin: Aerosol physiochemistry and optical properties during PEM Tropics A and B, *J. Geophys. Res.*, *108*(D2), 8236, 10.1029/2001JD001451, 2003.

Moxim, W. J., H. Levy II, and P. S. Kasibhatla, Simulated global tropospheric PAN: Its transport and impact on NOx, *J. Geophys. Res.*, *101*, 12,621–12,638, 1996.

Nesbitt, S. W., R. Zhang, and R. E. Orville, Seasonal and global NO_x production by lightning estimated from the Optical Transient Detector (OTD), *Tellus, Ser. B*, *52*, 1206–1215, 2000.

Olson, J. R., et al., Seasonal differences in the photochemistry of the South Pacific: A comparison of observations and model results from PEM-Tropics A and B, *J. Geophys. Res.*, *106*, 32,749–32,766, 2001.

Penner, J. E., D. J. Bergmann, J. J. Walton, D. Kinnison, M. J. Prather, D. Rotman, C. Price, K. E. Pickering, and S. Baughcum, An evaluation of upper tropospheric NO_x with two models, *J. Geophys. Res.*, *103*, 22,097–22,113, 1998.

Pickering, K. E., Y. Wang, W.-K. Tao, C. Price, and J.-F. Muller, Vertical distributions of lightning NO_x for use in regional and global chemical transport models, *J. Geophys. Res.*, *103*, 31,203–31,216, 1998.

Prather, M. J., Numerical advection by conservation of second-order moments, *J. Geophys. Res.*, *91*, 6613–6671, 1986.

Prather, M. J., and D. J. Jacob, A persistent imbalance in HO_x and NO_x photochemistry of the upper troposphere driven by deep tropical convection, *Geophys. Res. Lett.*, *24*, 3189–3192, 1997.

Price, C., and D. Rind, A simple lightning parameterization for calculating global lightning distributions, *J. Geophys. Res.*, *97*, 9919–9933, 1992.

Raper, J. L., M. M. Kleb, D. J. Jacob, D. D. Davis, R. E. Newell, H. E. Fuelberg, R. J. Bendura, J. M. Hoell, and R. J. McNeal, Pacific Exploratory Mission in the Tropical Pacific: PEM-Tropics B, March–April, 1999, *J. Geophys. Res.*, *106*, 32,401–32,426, 2001.

Ravetta, F., et al., Experimental evidence for the importance of convected methylhydroperoxide as a source of hydrogen oxide (HO_x) radicals in the tropical upper troposphere, *J. Geophys. Res.*, *106*, 32,709–32,716, 2001.

Ridley, B. A., et al., Is the Arctic surface layer a source and sink of NOx in winter/spring?, *J. Atmos. Chem.*, *36*, 1–22, 2000.

Riemer, D., et al., Observations of nonmethane hydrocarbons and oxygenated volatile organic compounds at a rural site in the southeastern United States, *J. Geophys. Res.*, *103*, 28,111–28,128, 1998.

Schultz, M. G., et al., On the origin of tropospheric ozone and NO_x over the tropical south Pacific, *J. Geophys. Res.*, *104*, 5829–5844, 1999.

Schultz, M. J., D. J. Jacob, J. D. Bradshaw, S. T. Sandholm, J. E. Dibb, R. W. Talbot, and H. B. Singh, Chemical NO_x budget in the upper troposphere over the tropical South Pacific, *J. Geophys. Res.*, *105*, 6669–6679, 2000.

Singh, H. B., et al., Latitudinal distribution of reactive nitrogen in the free troposphere over the Pacific Ocean in late winter/early spring, *J. Geophys. Res.*, *103*, 28,237–28,246, 1998.

Singh, H., Y. Chen, A. Staudt, D. Jacob, D. Blake, B. Heikes, and J. Snow, Evidence from the Pacific troposphere for large global sources of oxygenated organic compounds, *Nature*, *410*, 1078–1081, 2001.

Staudt, A. C., D. J. Jacob, J. A. Logan, D. Bachiochi, T. N. Krishnamurti, and G. W. Sachse, Continental sources, transoceanic transport, and interhemispheric exchange of carbon monoxide over the Pacific, *J. Geophys. Res.*, *106*, 32,571–32,590, 2001.

Staudt, A. C., D. J. Jacob, J. A. Logan, D. Bachiochi, T. N. Krishnamurti, and N. Poisson, Global chemical model analysis of biomass burning and lightning influences over the South Pacific in austral spring, *J. Geophys. Res.*, *107*(D14), 4200, doi:10.1029/2000JD000296, 2002.

Tabazadeh, A., O. B. Toon, and E. J. Jensen, A surface chemistry model for nonreactive trace gas adsorption on ice: Implications for nitric acid scavenging by cirrus, *Geophys. Res. Lett.*, *26*, 2211–2214, 1999.

Tabazadeh, A., M. Z. Jacobson, H. B. Singh, O. B. Toon, J. S. Lin, R. B. Chatfield, A. N. Thakur, R. W. Talbot, and J. E. Dibb, Nitric acid scavenging by mineral and biomass burning aerosols, *Geophys. Res. Lett.*, *25*, 4185–4188, 1998.

Talbot, R. W., J. E. Dibb, E. M. Scheuer, D. R. Blake, N. J. Blake, G. L. Gregory, G. W. Sachse, J. D. Bradshaw, S. T. Sandholm, and H. B. Singh, Influence of biomass combustion emissions on the distribution of acidic trace gases over the South Pacific basin during austral springtime, *J. Geophys. Res.*, *104*, 5623–5634, 1999.

Talbot, R. W., J. E. Dibb, E. M. Scheuer, J. D. Bradshaw, S. T. Sandholm, H. B. Singh, D. R. Blake, N. J. Blake, E. Atlas, and E. Flocke, Tropospheric reactive odd nitrogen over the South Pacific in austral springtime, *J. Geophys. Res.*, *105*, 6681–6694, 2000.

Tan, D., et al., OH and HO_2 in the remote tropical Pacific: Results from PEM-Tropics B, *J. Geophys. Res.*, *106*, 32,667–32,682, 2001.

Thakur, A. N., H. B. Singh, P. Mariani, Y. Chen, Y. Wang, D. J. Jacob, G. Brasseur, J.-F. Muller, and M. Lawrence, Distribution of reactive nitrogen species in the remote free troposphere: Data and model comparisons, *Atmos. Environ.*, *33*, 1403–1422, 1999.

Thompson, A. M., The oxidizing capacity of the Earth's atmosphere: Probable past and future changes, *Science*, *256*, 1157–1165, 1992.

Tie, X., R. Zhang, G. Brasseur, L. Emmons, and W. Lei, Effects of lightning on reactive nitrogen and nitrogen reservoir species in the troposphere, *J. Geophys. Res.*, *106*, 3167–3178, 2001.

Wang, Y., D. J. Jacob, and J. A. Logan, Global simulation of tropospheric O_3-NO_x-hydrocarbon chemistry, 1, Model formulation, *J. Geophys. Res.*, *103*, 10,713–10,726, 1998.

Wang, Y., et al., Factors controlling tropospheric O_3, OH, NO_x, and SO_2 over the tropical Pacific during PEM-Tropics B, *J. Geophys. Res.*, *106*, 32,733–32,748, 2001.

Wild, O., Z. Xin, and M. J. Prather, Fast-J: Accurate simulation of in- and below-cloud photolysis in global chemical models, *J. Atmos. Chem.*, *37*, 245–282, 2000.

Yevich, R., and J. A. Logan, An assesment of biofuel use and burning of agricultural waste in the developing world, *Global Biogeochem. Cycles*, *17*, doi:10.1029/2002GB001952, in press, 2003.

Zhang, Y., and G. R. Carmichael, The role of mineral aerosol in tropospheric chemistry in East Asia—A model study, *J. Appl. Meteorol.*, *38*, 353–366, 1999.

Zondlo, M. A., S. B. Barone, and M. A. Tolbert, Uptake of HNO_3 on ice under upper tropospheric conditions, *Geophys. Res. Lett.*, *24*, 1391–1394, 1997.

D. Bachiochi and T. N. Krishnamurti, Department of Meteorology, MC 4520, Florida State University, Tallahassee, FL 32306-4520, USA. (tnk@met.fsu.edu)

D. J. Jacob and J. A. Logan, Division of Engineering and Applied Sciences and Department of Earth and Planetary Sciences, Harvard University, Pierce Hall, 29 Oxford St., Cambridge, MA 02138, USA. (djj@io.harvard.edu; jal@io.harvard.edu)

F. Ravetta, Service d'Aéronomie du CNRS/IPSL, Université Paris 6 – Boîte 102, 4, Place Jussieu, F-75252 Paris Cedex 05, France. (francois.ravetta@aero.jussieu.fr)

B. Ridley, National Center for Atmospheric Research, P. O. Box 3000, Boulder, CO 80307, USA. (ridley@acd.ucar.edu)

S. Sandholm, School of Earth and Atmospheric Sciences, Georgia Institute of Technology, Baker Bldg Rm 107, Atlanta, GA 30332, USA. (ss27@prism.gatech.edu)

H. B. Singh, NASA Ames Research Center, MS 245 5, 21 Langley Blvd., Moffett Field, CA 94035, USA. (hsingh@mail.arc.nasa.gov)

A. C. Staudt, Board on Atmospheric Sciences and Climate, The National Academies/National Research Council, 500 5th Street, N.W., Washington, DC 20001, USA. (astaudt@nas.edu)

R. Talbot, Complex Systems Research Center/Institute for the Study of Earth, Oceans, and Space, University of New Hampshire, 39 College Road/Morse Hall, Durham, NH 03824-3525, USA. (robert.talbot@unh.edu)

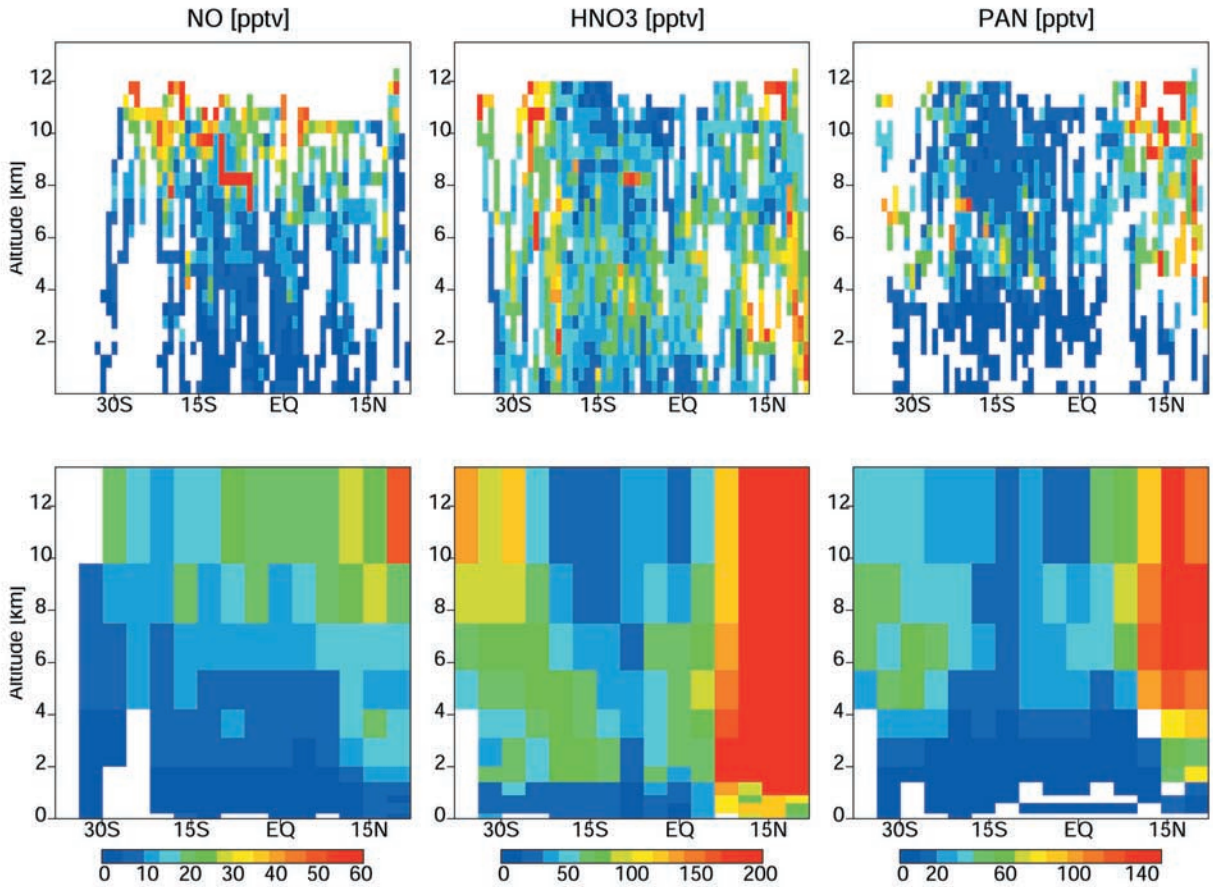

Figure 2. Concentrations of NO, HNO_3, and PAN during PEM-Tropics B plotted as a function of altitude and latitude (see Figure 1). (top) Observations averaged across 165°E–100°W longitude and into 0.5° latitude by 0.5 km altitude boxes. The NO observations have been restricted to those obtained between 0900 and 1500 LT. (bottom) Simulated concentrations of NO, HNO_3, and PAN sampled for the day and location of the PEM-Tropics B flights. The model values are sampled along the flight tracks and for the flight days, and the results are averaged across 165°E–100°W longitude and for the model resolution of 4° latitude. The simulated NO is the average of daytime (0900 to 1500 LT) concentrations, while HNO_3 and PAN are 24-hour averages. DC-8 flight 22, which followed the western coast of Central America from Costa Rica to California, is not included.

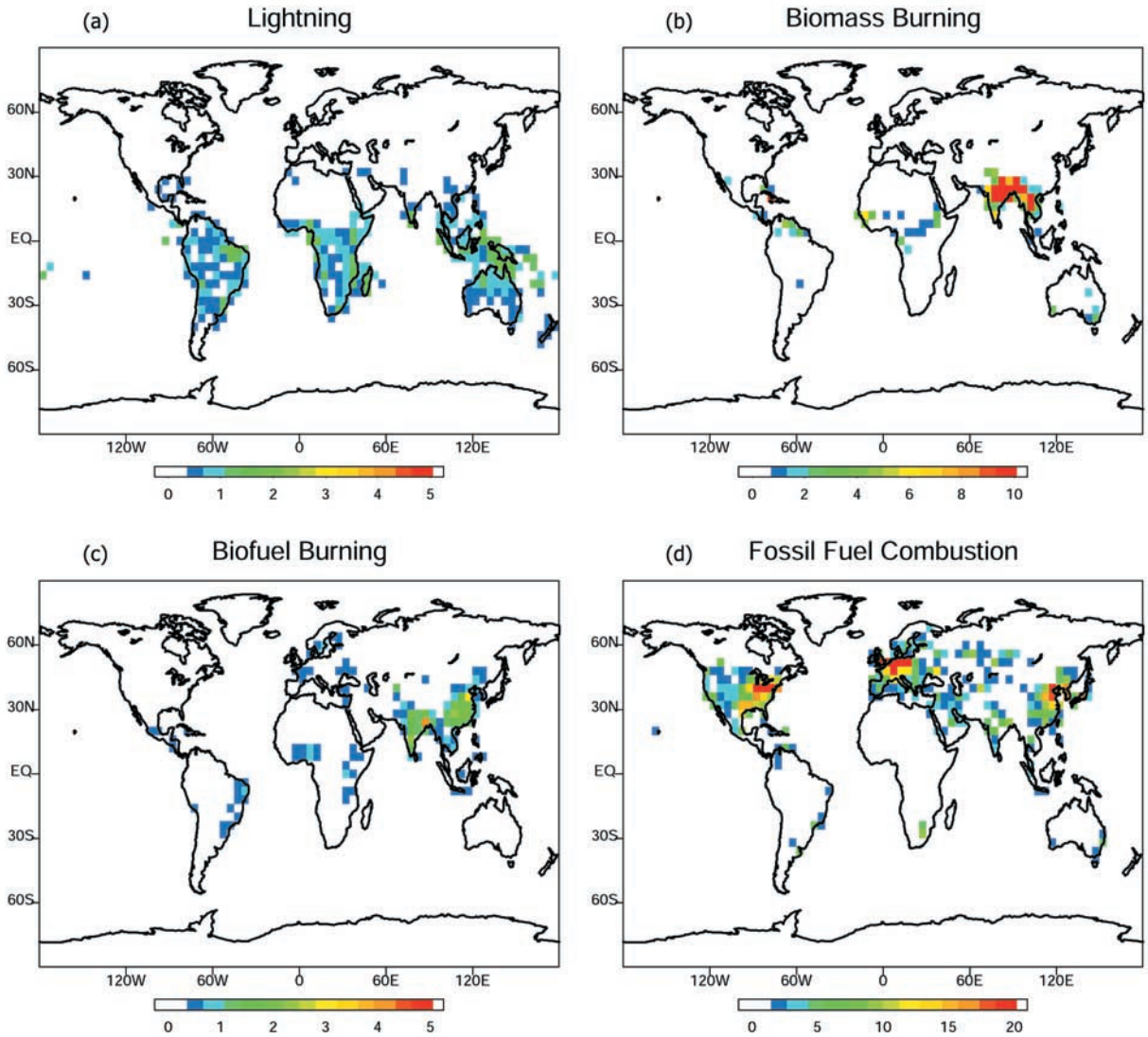

Figure 5. Distribution of NO_x emissions (units) used in the model for (a) lightning, (b) biomass burning, (c) biofuel burning, and (d) fossil fuel combustion. Values are averages for the PEM-Tropics B time period (1 March to 19 April 1999).